NUMERICAL ANALYSIS OF ROCK BLASTING

By Kshitiz Joshi

WORD COUNT 12516
TIME SUBMITTED 24-DEC-2023 09:49PM
PAPER ID 105714271

TRIBHUVAN UNIVERSITY
INSTITUTE OF ENGINEERING
PULCHOWK CAMPUS

Roll No.: PUL078MSGTE008.

NUMERICAL ANALYSIS OF ROCK BLASTING

by

Kshitiz Joshi.

A THESIS

SUBMITTED TO THE DEPARTMENT OF CIVIL
ENGINEERING IN PARTIAL FULFILLMENT OF THE
REQUIREMENTS FOR THE
DEGREE OF MASTER OF SCIENCE IN GEOTECHNICAL ENGINEERING

DEPARTMENT OF CIVIL ENGINEERING
LALITPUR, NEPAL

COPYRIGHT

TRIBHUVAN UNIVERSITY
INSTITUTE OF ENGINEERING
PULCHOWK CAMPUS
DEPARTMENT OF CIVIL ENGINEERING

APPROVAL PAGE

The undersigned certify that they have read, and recommended to the Institute of Engineering for acceptance, a thesis entitled **"Numerical Analysis of Rock Blasting"** submitted by Mr. Kshitiz Joshi (078/MSGtE/008) in partial fulfillment of the requirements for the degree of Master of Science in Geotechnical Engineering.

……..

Supervisor: Dr. Santosh Kumar Yadav
Assistant Professor
Pulchowk Campus

……..……

External Examiner: Er. Prabhat Kumar Jha
Superintendent Engineer
Department of Roads

……

Program Coordinator: Dr. Santosh Kumar Yadav
M.Sc. Program in Geotechnical Engineering
Department of Civil Engineering
Pulchowk Campus

December,2023

ABSTRACT

Rock blasting serves as a pivotal tool in mining and civil engineering, specifically for the purpose of rock removal. It is an efficient alternative to tunnel boring machines, particularly in the context of tunnel excavation through challenging geological formations. The detonation of explosive materials triggers the rapid generation of highly pressurized gas within an extremely short time span, thereby exerting pressures on the rock wall that can reach magnitudes on the order of several Gigapascals.

Examining the impacts of rock blasting through scaled or full-size experiments is both costly and time intensive. Conversely, employing numerical methods based on robust mechanical principles, validated against experimental data, emerges as a promising avenue for unveiling the fracture processes induced by blasting. The intricate nature of the response of rock masses to explosive loads, owing to factors such as anisotropy, nonlinearity, variability in mechanical properties of rock materials, and the simultaneous presence of solid, liquid, and gas phases, adds complexity to the analysis.

Prior investigations into rock blasting damage and blast-induced vibration have employed various methods, including theoretical analysis, field tests, numerical simulations, and model tests. Notably, numerical simulation stands out as a prevalent approach in the study of blasting processes.

The hydrocode LS Dyna has been used for numerical simulation of the rock blasting process. Johnson-Holmquist 2 (JH-2) damage model as well as Riedel-Hiermaier-Thoma (RHT) constitutive model, combined with Arbitrary Lagrangian Eulerian Model (ALE) Model has been used. The crack patterns generated by both the numerical models were found in close conformity with the results of the lab scale experiments performed with Barre Granite. However, RHT model was found to be more efficient in modeling rock interaction with explosives compared to the JH-2 model.

After the calibration and validation of the model with the lab experiments, two separate models were made to understand the propagation of cracks and pressure distribution due to blasting. The first model was done to understand the effect of decoupling

coefficient on the blasting behavior of the Barre Granite. The second model was created to understand the effect of delay time and spacing of explosives on the crack propagation. The effect of decoupling coefficient was found to be found that with the increase in the coefficient, the damage area reduced and the pressure in the surroundings reduced. The energy dissipation was more when air was used as decoupling media compared to water.

Thereafter, the effect of delay timing of explosives on rock fragmentation was studied. It was found that there is an optimum delay time for the different borehole spacings which leads to the highest amount of fragmentation. Furthermore, the effect of spacing of explosives was found. With the increase in spacing, the damage in the region parallel to the explosives increased whereas in the region perpendicular to the placement of explosives decreased. Keywords: Rock Blasting, LS Dyna, JH-2 model, Banadaki Experiment, Decoupling ratio, Explosive Spacing, Delay Timing.

ACKNOWLEDGEMENTS

I want to express my deepest and sincere gratitude to my supervisor, Assistant Professor Dr. Santosh Kumar Yadav, for his invaluable guidance and support over the past 12 months, particularly during the preparation of this thesis. The journey of the last year has been a significant undertaking, and without his motivation and expert guidance, it would not have been as fulfilling and educational. My heartfelt thanks also go to Associate Professor Indra Prasad Acharya, Assistant Professor Bhim Kumar Dahal, Assistant Professor Ram Chandra Tiwari, and the entire Department of Geotechnical Engineering at Pulchowk Campus for providing crucial opportunities that enriched my exposure.

My gratitude also extends to the dedicated staff of the M.Sc. Program in Geotechnical Engineering for their support and for granting me access to the facilities essential for my research.

TABLE OF CONTENTS

Contents

TABLE OF FIGURES

LIST OF TABLES

1. INTRODUCTION

1.1 Background

Rock blasting is extensively used in civil engineering projects. In the hilly terrain of Nepal, it has been used for a long time in road construction. To fulfill the enormous hydropower potential of Nepal, several hydropower projects are being constructed. Tunneling is a key part of these projects. More than 200 kms of hydropower tunnels have been constructed till date. In the road sector as well, the tunnel age has begun. Nagdhunga tunnel is near completion whereas Siddhababa road tunnel is in the construction phase with several new tunnel projects in the pipeline. Drill and blast is very common method of tunneling in Nepal. Apart from a few projects constructed with the Tunnel Boring Machines (TBMs), majority of the tunnels have been constructed with drill and blast methodology.

In the drill and blast method of tunneling, the tunnel advance is made through drilling several holes in the rock, loading them with explosives, detonating the explosives and subsequent removal of rocks and muck. The variables involved in this method include type of rock, type of explosives, method of cutting such as parallel cut, wedge cut, powder factor, detonation time and delays, burden, hole diameter and decoupling ratio. Precise and detailed calculations are required to optimize the blast efficiency to obtain required cross section through blasting. In other words, underbreak and overbreak both pose problems to the working contractors as well as client.

In this context, very few research have been made to understand and study the blasting phenomenon in rocks in Nepal. The experimental analysis is extremely complicated due to difficulty in obtaining information from the blasting due to transient nature of the blast as well as safety issues during blasting. However, it is imperative to understand the blasting process and the manner of crack propagation and destruction process of rocks subject to the blast loading.

Numerical analysis is a very effective method to understand and simulate the rock blasting phenomena. Several software programs such as Abaqus, LS Dyna, FLAC can be used to simulate the process. Using numerical analysis, parametric analysis can be done to understand the effects of several variables on the whole blasting process. The study of the blasting process using simulation can improve the blasting efficiency as well as the whole process of blasting with the aim of improving the

blasting design in the future.

1.2 Statement of Problem

To better understand the explosion process, it is necessary to accurately simulate the rock explosion. Several attempts have been made to numerically model the blasting process. It is important to understand the Constitutive models used for blasting process, especially for rocks and explosives. For rocks, the constitutive model must be able to accurately depict the brittle nature of the rocks. Furthermore, the Fluid Structure interaction in the form of interaction of blasting waves with the rocks and subsequent damage must be accurately modelled. Various methods of modeling the rocks and explosives in the form of Lagrangian, Eulerian and Arbitrary Lagrangian Eulerian (ALE) have been used. Similarly, some parameters of blasting such as effect of decoupling ratio on blasting using the selected constitutive model needs to be studied. Furthermore, the effect of delay time and spacing of blastholes on the damage also needs further analysis.

1.3 Objective

- To establish suitable numerical model validated against a numerical model of case study and laboratory measurement.
- To determine the effectiveness of constitutive models of rock for simulating blasting.
- To understand the crack propagation process in blasting.
- To understand the pressure distribution during blasting.
- To determine the effect of decoupling coefficient and various decoupling media in blasting.
- To determine the effect of spacing of explosives in damage propagation.
- To determine the effect of delay time of detonation of explosives in rock damage.

1.4 Scope and limitation of Study

- It is carried out based on the laboratory experiment on intact rock. It doesn't consider the effect of joints in the rock.
- The study is done on the Barre Granite sample used in the laboratory experiments and the parameters for model determined from another study.

- The analysis is carried out in LS Dyna Software. There was difficulty in meshing to create smooth shaped mesh around explosives.

1.5 Methodology

The thesis studies the numerical simulation of blasting on the rock. Due to the limitation in obtaining the field data to validate the numerical model, a laboratory test conducted by (Banadaki, 2010) on Barre Granite has been used for numerical validation. The crack patterns in the rock specimen as well as pressure measured in various points have been used to calibrate and validate the model. After validation, the same material as well as parameters are used to simulate rock blasting under other conditions. Firstly, the effect of decoupling coefficient on the damage and crack propagation in the rock is studied. Furthermore, the effect of spacing of blastholes on damage of rock and pattern of crack propagation is further studied. The materials used were the same as the ones used for experimental studies.

1.6 Content of this thesis

The chapter first introduces the overall thesis works. Chapter two contains the methodology employed and some literature review about the concepts involved in the numerical simulation of blasting, including information about the Hydrocodes, Lagrangian, Eulerian and ALE formulation, methodologies to simulate blast in FEM. In Chapter 3, the detail about the experimental result is provided. A numerical model is made to validate the results against the experimental results. Two constitutive models are used for two separate numerical models. The performance and effectiveness of both the constitutive models is compared and the numerical model is calibrated against the experimental measurements. Chapter 4 contains numerical simulation of blasting for different decoupling ratios. The damage in the rock for different decoupling ratios are compared and blasthole pressures for different cases are observed. Comparison between decoupling media of air and water is made. Chapter 5 contains the numerical simulation in which the rock damage is compared for different delay time of explosives detonation and different spacing of blastholes. Chapter 6 contains conclusions.

2. METHODOLOGY EMPLOYED

2.1 HYDROCODES

Numerical calculations play a pivotal role in unraveling the intricate mechanisms underlying highly transient events, such as explosions and impacts. Wave propagation codes, commonly known as hydrocodes, have been instrumental in tackling nonlinear challenges across solid, liquid, and gas dynamics.

The solution to transient problems involves applying the principles of mass, momentum, and energy conservation, along with appropriate initial and boundary conditions. Modeling the material's behavior is crucial, and hydrocodes often employ the division of the total stress tensor into a hydrostatic pressure, uniform in all directions, and a deviating stress tensor. Volume changes are captured through an equation of state, relating pressure to density or specific volume, while shear strength is modeled using a strength model, often determined by the bending stress tensor at failure.

Explicit time integration schemes are commonly employed in hydrocodes to calculate state variables efficiently at the current time point. While these schemes offer high calculation efficiency by bypassing mass or stiffness matrix calculations, their stability is constrained, with stress propagation limited by the size of the smallest element in each time step.

Numerous commercial hydrocodes, such as AUTODYN, ABAQUS, and LS-DYNA, cater to simulating nonlinear dynamic problems like high-speed impact testing and the effects of explosives on structures. ANSYS AUTODYN, developed by Century Dynamics, stands out as a comprehensive hydrocode with a rich material model library covering metals, concrete, soil, ceramics, composites, and explosives. LS-DYNA, another widely used hydrocode, offers a multiphysics approach with various descriptions like Lagrangian, Eulerian, Arbitrary Lagrangian Eulerian (ALE), and Meshfree for simulating complex scenarios such as penetration, blast loading, fluid-structure interaction, and crashworthiness. LS-DYNA, derived from DYNA3D, is especially favored in the automotive industry for crashworthiness calculations and has found applications in researching dynamic tensile fractures of rocks.

ABQUS/EXPLICIT, yet another explicit solver, excels in simulating high-speed dynamic events, complex contact problems, and highly nonlinear quasi-static scenarios with material degradation and failure. However, it uses a non-multi-material ALE description, limiting its capability in handling multi-material problems. For the dynamic behavior of rock-type materials under blast loads, ABAQUS often utilizes blast pressure profiles obtained from other software or analytical models.

For the purpose of this study, LS DYNA has been used.

2.2 ARBITRARY LAGRANGIAN EULERIAN:

The LS-DYNA program incorporates three distinct algorithms: Lagrangian, Eulerian, and Arbitrary Lagrangian Eulerian (ALE). The Lagrangian algorithm is well-suited for analyzing material deformation processes and tracking the time history of substance particles. It accurately captures displacements and deformations, making it primarily employed for analyzing the stress and strain in solid structures. However, a drawback lies in its tendency to produce severe mesh twist deformations or negative volumes in scenarios involving large displacements and deformations, leading to potential calculation stoppages due to numerical errors.

On the other hand, the Eulerian algorithm maintains a fixed mesh system independent of the object being analyzed, preventing severe mesh twist deformations. This algorithm is effective in analyzing fluid flow, as well as the diffusion and mixing of gases. Nevertheless, it faces challenges in obtaining the physical ratio occupied by the material in the mesh, and the entire material being described must be covered by the element mesh.

The Arbitrary Lagrangian Eulerian (ALE) algorithm addresses the limitations of both Lagrangian and Eulerian algorithms while capitalizing on their strengths. By utilizing mass conservation, momentum conservation, and additional momentum conservation equations, the ALE algorithm overcomes issues related to interrupted numerical calculations caused by mesh deformation. Simultaneously, it allows for

effective control and tracking of structural boundary movement. This algorithm is frequently employed in real-time dynamic analyses of coupled fluids and solids, providing a versatile solution for complex simulations.

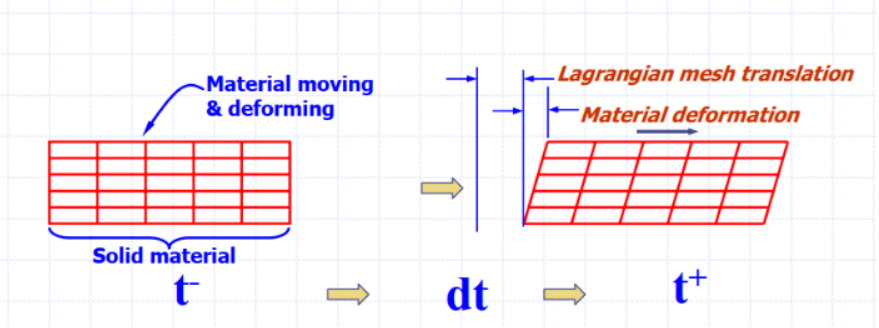

Figure 1 Lagrangian mesh

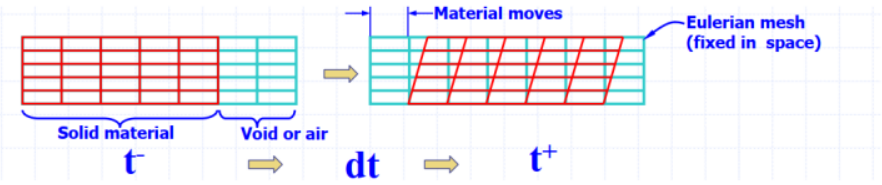

Figure 2 Eulerian Mesh

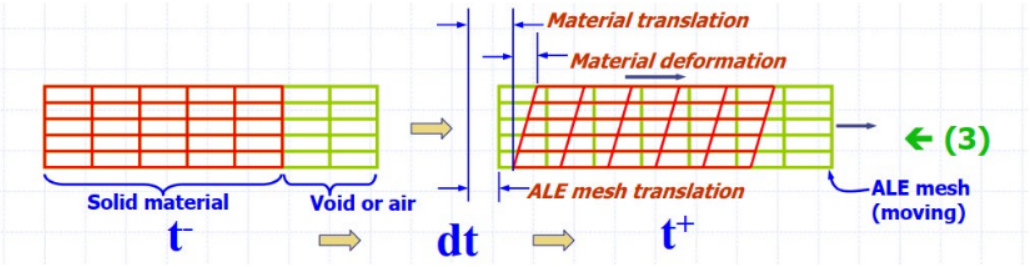

Figure 3 ALE Mesh

2.3 SPH Method:

In meshfree methods, nodes or particles are affixed to the material, constituting Lagrangian descriptions. Unlike grid-based methods, meshfree approaches lack connectivity between nodes or particles, yet they deliver precise solutions for integral and differential equations. Smoothed Particle Hydrodynamics (SPH) stands out as a widely utilized meshfree method in both solid and fluid mechanics.

SPH, a meshfree computational Lagrangian hydrodynamic particle method, originated approximately three decades ago in the realm of astrophysics, initially designed for simulating the interactions of fluid masses in a vacuum without boundaries. Over time, it evolved into a deterministic mesh-free particle method and found application in continuum solid and fluid mechanics. SPH is particularly adept

at handling solid mechanics problems marked by large deformations and fragmentation. Its mathematical foundation lies in interpolation theory, employing kernel approximation to a function that remains suitably smooth even for higher-order derivatives, thereby ensuring stable and accurate results. However, during its initial application beyond astrophysics, SPH encountered challenges related to enforcing finite boundary conditions.

SPH serves as a robust numerical tool for modeling problems characterized by significant distortions and deformations. Notably, SPH avoids mesh tangling and hourglassing effects associated with conventional Lagrangian meshes. Therefore, SPH particles are strategically employed in scenarios where large deformation or severe material failure is expected in the near-field domain, while finite element (FE) meshes are utilized in instances where intermediate or small deformations are anticipated in far-field domains.

Although SPH comes with a higher computational cost, the coupled SPH-FE approach mitigates this demand, offering a balanced solution that leverages the strengths of both methods.

$$\frac{d\rho}{dt} = -\rho\frac{\partial v_i}{\partial x_i};\ \frac{dv_i}{dt} = \frac{1}{\rho}\frac{\partial \sigma_{ij}}{\partial x_j};\ \frac{dE}{dt} = \frac{\sigma_{ij}}{\rho}\frac{\partial v_i}{\partial x_j}$$

$$\frac{\partial \rho_p}{\partial t} = \sum_{q=1}^{N} m_q v_{pq}\frac{\partial W_{pq}}{\partial X_p},$$

$$\frac{\partial v_p}{\partial t} = \sum_{q=1}^{N} m_q\left(\frac{\sigma_p}{\rho^2{}_p} + \frac{\sigma_q}{\rho^2{}_q}\right)\frac{\partial W_{pq}}{\partial X_p},$$

$$\frac{\partial E_p}{\partial t} = \sum_{q=1}^{N} m_q\left(\frac{\sigma_p \sigma_q}{\rho_p \rho_q}\right)v_{pq}\frac{\partial W_{pq}}{\partial X_p},$$

Where, $\boldsymbol{\sigma}$ is the stress, v is the velocity, ij are indexes of components, E is the internal energy, m is the mass of the particle, W is a kernel function, N is the number of particles within the smoothing length and p and q are the indexes denoting different particles.

The equations are solved by:

$$\langle f \rangle (x) = \int f(x')W(x - x', h)dx' = \sum_{q=1}^{N} f(x_q)W(x - x_q, h)\Delta V_q$$

Where <f> is the function interpolation; x is the vector defining the particle's position; h is the maximum distance between particles (smoothing length) and W is

the kernel function.

2.4 Data Manipulation:

LS-DYNA provides two formats for analyzing output data: binary files and ASCII. Binary files, including d3plot, d3thdt, d3dump, and interface force files, store finite element response information from the model. The recording interval for binary files can be customized, ranging from 250 microseconds to 1000 microseconds, depending on the desired precision for capturing peak measurements and tunnel responses during explosive events.

For processing LS-DYNA output and visualizing three-dimensional responses, LS-PrePost is utilized. LS-PrePost reads various results data files such as d3plot, intfor, and all ASCII time history data files. Its visualization capabilities include dynamic animations and color contour images on meshes, representing acceleration, velocity, displacement, and element pressure time history data. Additionally, LS-PrePost computes various parameters, including strains, bending moments, and reaction forces along constrained boundaries.

Binary d3dump files are automatically generated upon normal termination and serve the purpose of restarting the model by eliminating redundant elements. This feature enhances efficiency and allows the continuation of simulations from a specific point.

2.5 Keywords used in LS DYNA to simulate explosions:

MAT_JOHNSON_HOLMQUIST_CERAMICS:

MAT_JOHNSON_HOLMQUIST_CERAMICS, known as the Johnson-Holmquist Ceramic (JH-2) material model, is employed in LS-DYNA to replicate the behavior of brittle materials like ceramics under high strain rates. This model is an extension of the Johnson-Holmquist Concrete (JH-1) material model and is specifically designed to simulate how ceramics respond to dynamic loading conditions.

The JH-2 model addresses aspects such as brittle failure, strain rate effects, and damage evolution in ceramic materials. It integrates the Johnson-Cook constitutive model for the plasticity component and includes criteria for strength and failure in ceramics. The essential material properties required for implementing the JH-2

model encompass density, elastic properties of the material, strength parameters, failure parameters, and strain rate sensitivity.

MAT_HIGH_EXPLOSIVE_BURN

High explosive burn pertains to the rapid combustion or swift chemical reaction of high explosives, leading to the release of energy in the form of heat, pressure, and the production of hot gases. When high explosives undergo combustion, it typically involves a speedy exothermic reaction that travels through the material, causing rapid decomposition and the liberation of a significant amount of energy.

The behavior of high explosives during burning is influenced by several factors, including the specific consumption of the explosive material, its physical characteristics, and the conditions under which the burn takes place. Modeling the burn is a challenging task that often necessitates specialized models.

Within LS-DYNA, the MAT_HIGH-EXPLOSIVE_BURN feature enables users to define properties of the explosive material, such as detonation velocity, reaction rate, energy release, and the pressure-volume relationship. Detonation velocity represents the speed at which the detonation wave spreads through the explosive material, while the Chapman-Jouguet Pressure denotes the pressure at which the detonation velocity reaches its maximum.

EOS_JWL

34

The Jones-Wilkins-Lee (JWL) equation of state finds application in modeling the dynamics of high explosives, especially in hydrodynamic simulations. It characterizes the pressure-volume correlation of the explosive material based on its specific energy and detonation velocity.

Description of parameters:

C0= Initial sound speed of the material.

A, B: Parameters controlling the shock Hugonoit curve

R1,R2,R3: Parameters controlling the release isentrope.

T1,T2, T3, T4, T5: Parameters controlling the time delay behavior.

These parameters collectively define the intricate relationship between pressure and

volume for high explosives in dynamic scenarios. The JWL equation of state is a valuable tool for accurately simulating and understanding the behavior of high explosives under various conditions.

SECTION_SOLID:

The solid element's section definition serves the purpose of allocating material properties and attributes to designated regions or segments within the solid mesh. This definition is instrumental in specifying crucial characteristics, including material type, thickness, orientation, and integration type for solid elements. Essentially, it plays a pivotal role in outlining the anticipated behavior and response of the solid elements throughout the simulation process. By utilizing the section definition, engineers and analysts can precisely tailor the material considerations for distinct portions of the solid model, contributing to more accurate and detailed simulations of the structural response.

The term "Elform" refers to element formulation parameters, which play a crucial role in determining the integration and shape functions applied within elements in a simulation. Specifically, when elform is set to -2, it signifies the use of the Hourglass Control formulation for solid elements.

The Hourglass Control element formulation is employed to address and minimize hourglass-type deformations that may arise in certain types of elements, especially when utilizing reduced or selective reduced integration methods. These deformations can impact the accuracy and stability of simulations, and the Hourglass Control formulation serves as a technique to mitigate such undesired effects. By adjusting the elform parameter, users can select the appropriate formulation to enhance the performance and reliability of the simulation, particularly when dealing with solid elements.

SECTION_SPH:

It is used to define the material properties and characteristics for Smooth Particle Hydrodynamics (SPH) elements.

HOURGLASS_HOURGLASS

The term "hourglass" refers to a specific type of numerical instability or undesirable deformation pattern that can manifest in certain finite element models. Hourglassing poses a risk of generating unrealistic deformations, potentially yielding inaccurate

results if not effectively controlled. This phenomenon occurs when a mesh or element formulation permits local deformations that do not actively contribute to the overall strain energy. These localized deformations can lead to artificial energy dissipation, resulting in an inaccurate representation of the material's behavior in the simulation. Proper control mechanisms and formulation adjustments are essential to mitigate hourglassing and ensure the fidelity of finite element simulations.

CONTACT_AUTOMATIC_NODES_TO_SURFACE

The automatic contact algorithm is a feature that enables the definition of contact interactions between nodes and surfaces without the explicit specification of contact surfaces. This functionality is implemented through the CONTACT_AUTOMATIC_NODES_TO_SURFACE keyword. With this keyword, the algorithm automatically identifies and establishes contact between nodes and surfaces during the analysis, relying on the proximity of these entities in the simulation.

In simpler terms, the CONTACT_AUTOMATIC_NODES_TO_SURFACE keyword allows the software to autonomously detect and handle contact interactions, streamlining the modeling process by eliminating the need for manually defining contact surfaces. This can enhance efficiency and reduce the complexity of setting up contact interactions in simulations.

We must identify the slave element and the master element in this keyword.

In the context of contact modeling in finite element analysis, the "Slave element" is the element that undergoes deformations and makes contact with other elements. The term "Slave" indicates that this element is influenced or controlled by the contact conditions established with another element, known as the "Master element." The Slave element is responsible for transmitting contact forces to the Master element, which, in turn, reacts to these forces and influences the behavior of the Slave element.

In summary, the Slave element is the one experiencing deformations and contacting other elements, and it plays a crucial role in the overall contact interactions within a finite element simulation. The distinction between Slave and Master elements helps define the contact relationships and ensures accurate representation of the physical interactions between different parts of a model.

In the context of contact modeling in finite element analysis, the "Master element" is the element that the Slave element contacts. The Master element is typically a rigid

or deformable element that serves as the receiving end of contact forces transmitted by the Slave element.

The Master-Slave relationship is a fundamental concept in contact analysis. The Master element is not influenced by the contact conditions; rather, it reacts to the forces and interactions initiated by the Slave element. This relationship helps simulate the contact and interaction between different parts of a model accurately, enabling the simulation of realistic physical behaviors in a wide range of engineering applications.

INITIAL_DETONATION

This keyword helps to define the detonating element and coordinates of the point of explosion.

CONTROL_TERMINATION

This keyword is used to specify the termination criteria for simulation. It allows to define the conditions that determine when the analysis should stop based on time criteria.

3. COMPARISON OF EFFECTIVENESS OF JH-2 AND RHT CONSTITUTIVE MODELS TO SIMULATE ROCK BLASTING.

In a lab investigation carried out by (Banadaki, 2010), a Barre granite rock specimen with dimensions of 14.4 cm in diameter and 15 cm in height was employed. A core hole was drilled at the center of the specimen, accommodating an explosive apparatus enclosed within a copper tube with an external diameter of 6.45 mm. The hole was filled with air, a polyethylene covering, and Pentaerythritol tetranitrate (PETN).

The materials involved had varying dimensions, with the rock sample having a diameter of 14.4 cm, the borehole measuring 6.45 mm, air occupying 5.24 mm, the polyethylene sheath having a diameter of 4.5 mm, and PETN measuring 1.65 mm. To prevent gas penetration into cracks, the copper tube was securely placed in the borehole, and the explosive was initiated from the top of the borehole.

(Wang, 2018) and (Li, 2023) duplicated the Banadaki experiment using the LS Dyna Hydrocode. In this thesis, the FEM LS Dyna was used to reproduce both the lab experiment conducted by (Banadaki, 2010) and the numerical simulations conducted by (Wang, 2018) and (Li, 2023).

The cylindrical sample was simulated using the JH-2 constitutive law proposed by (Wang, 2018) and the RHT model proposed by (Li, 2023). To effectively address issues involving substantial deformation, the ALE (Arbitrary Lagrangian-Eulerian) methodology was adopted instead of the traditional Lagrangian Finite Element Method (FEM). The ALE multi-material formulation was specifically utilized. In the Arbitrary Lagrangian-Eulerian (ALE) formulation, the mesh is granted the freedom to undergo independent movement, separate from the material flow. Additionally, each element can accommodate the blend of two or more distinct materials.

Figure 4 Cylindrical sample used by (Banadaki, 2010)

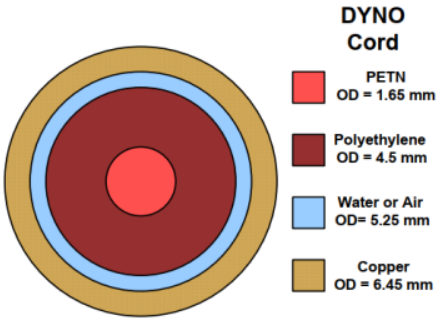

Figure 5 Plan of the cylindrical sample used by (Banadaki, 2010)

Methodology Employed:

Two models were created for simulating the materials as per the Banadaki experiment. The first model was created with the material parameters used by Wang (2018) with JH-2 model and the second model was created with the material parameters used by Li (2022) with RHT model. The dimensions of the rock, copper, Polyethylene, air and PETN were the same as that of the experiment. The mesh size used was 1mm x 1mm x 5 mm for all the elements. The rock and copper were modelled using Lagrangian formulation. The PETN, air, Polyethylene was modelled using the ALE.

The deformation of materials was simulated in two stages, initially with the solid mesh deforming according to the Lagrangian approach. Subsequently, the state variable of the Lagrangian element was conveyed to the entire ALE (Arbitrary Lagrangian-Eulerian) mesh space. The ALE method was chosen as a fluid-structure

interaction (FSI) technique for facilitating the coupling of the explosive and solid . In the applied methodology, copper and rock were represented with the material model of Lagrange, whereas the other four materials used ALE.

The boundaries of the materials incorporated merged nodes, forming ALE layers that constituted an ALE multi-material group (AMMG). Within this framework, ALE materials could flow across the meshes of all ALE components without inducing mesh deformation, following advection algorithms for the flow. Fluid-structure interaction (FSI) was simulated through a coupling algorithm utilizing the "Constrained_Lagrange_in_Solid" keyword in LS-DYNA, capturing the interaction between materials. The initiation of the material occurred at time t=0 from the base of the sample, mirroring the experimental conditions. The simulation concluded after 1x10^(-4) seconds.

For the Lagrangian elements, Hourglass control type 3 was applied, while control type 1 was implemented for the ALE elements. Solid Section Element Formulation 1 was used for the Lagrangian elements, and Solid Section Formulation 11 was employed to simulate the ALE elements. Free boundary conditions were utilized to align with the experimental setup. The model was configured in SI units, employing meters for length, seconds for time, and kilograms for mass.

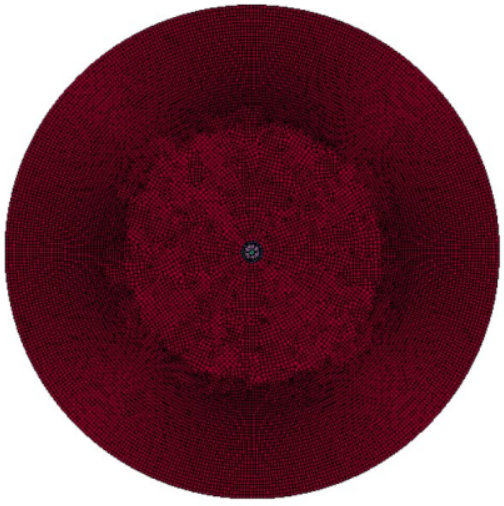

Figure 6 Plan view of the model created using LS DYNA

Figure 7 View of the Model created using LS DYNA

JH-2 Model for Rock:

The JH-2 plasticity damage model is commonly employed in the simulation of rocks and other materials exhibiting brittleness. It was initially introduced by (Johnson, 1992). Nevertheless, it lacks the ability for gradual strain softening, which diminishes its suitability for certain ceramic materials. In response to this constraint, the modified JH-2 model was introduced, evolving from the groundwork laid by the original JH-1 formulation.

Strength:

$$\sigma^* = {\sigma_i}^* - D({\sigma_i}^* - {\sigma_f}^*)$$

Where ${\sigma_i}^*$ is the normalized intact equivalent stress, ${\sigma_f}^*$ is the normalized fracture stress and D is the damage coefficient.

The normalized equivalent stress $(\sigma^*, {\sigma_i}^*, {\sigma_f}^*)$ have the general form:

$$\sigma^* = \frac{\sigma}{\sigma_{HEL}}$$

Where,

σ is the actual equivalent stress and σ_{HEL} is the equivalent stress at the Hugonoit elastic limit (HEL) and the normalized fracture strength is given by:

$${\sigma_f}^* = B\,({P^*})^M(1 + C.\ln \varepsilon^*)$$

The normalized pressure is $P^* = P/P_{HEL}$, where P is the actual pressure and P_{HEL} is the pressure at the Hugonoit Elastic Limit.

Damage:

The damage is expressed as:

$$D = \sum \Delta\varepsilon^p / \varepsilon_f^p$$

Where, $\Delta\varepsilon^p$ is the plastic strain during a cycle of integration and $\varepsilon_f^p = f(P)$ is the plastic strain to fracture under a constant pressure, P. The specific expression is:

$$\varepsilon_f^p = D_1(P^* + T^*)^{D_2}$$

Where, D_1 and D_2 are constants.

Equation of State:

The hydrostatic pressure before fracture initiates can be enumerated as:

$$P = K_1.\mu + K_2.\mu^2 + K_3.\mu^3$$

The parameters used for the numerical model were as per (Wang, 2018)

S.No.	Parameter	Details
1.	Density	2660
2.	Shear Modulus (G)	21.9e9
3.	Intact Strength Coefficient, A	1.25
4.	Fractured Strength Coefficient, B	0.68
5.	Strain rate Coefficient, C	0.005
6.	Fractured Strength exponent, M	0.83
7.	Intact Strength exponent, N	0.68
8.	Maximum Tensile strength, T	57e6
9.	Hugoniot Elastic Limit, (HEL) (Pa)	4.5e9
10.	HEL Pressure, Pa	2.93e9
11.	Bulk Factor	1.0
12.	Damage coefficient, D1	0.008
13.	Damage coefficient, D2	0.44
14.	Bulk modulus, K1 (Pa)	25.7e9
15.	Second pressure coefficient, K2 (Pa)	-386e9

16.	Third Pressure coefficient, K3 (Pa)	12800e9
17.	Maximum normalized fractured strength	0.16

Table 1 Properties of Barre Granite, JH-2 model, Wang (2018)

RHT Model:

Riedel-Hiermaier- Thoma Model (RHT) stands as an advanced damage plasticity model designed for brittle materials, initially proposed by (Riedel W, 1999) to analyze the dynamic loading of concrete. Subsequently, it was incorporated into the LS-DYNA code by (Borrvall T, 2011) for the modeling of more brittle materials. The RHT model incorporates three limit surfaces, namely the failure surface, yield surface, and residual surface, to characterize the material strength model. It is crucial to highlight that when the stress reaches the residual surface, as discussed by (Borrvall T, 2011), the material is fully damaged, and the strength is determined by the properties of the residual surface.

In the RHT model, the damage degree is defined as follows:

$$D_f = \sum \frac{\Delta\varepsilon^p}{\varepsilon^f}$$

Where, $\Delta\varepsilon^p$ is the accumulated plastic strain and ε^f is the failure strain written as:

$$\varepsilon^f = D_1\left(\frac{p}{f_c'} - \frac{p_{spall}}{f_c'}\right)^{D_2}$$

in which D_1 and D_2 are the initial damage parameters given by the user; p and p_{spall} are pressure and spalling strength respectively, f'c is the uniaxial compressive strength. In the Banadaki experiment, the mass density of the Barre Granite was 2660 kg/m3, Elastic Shear Modulus was 20.28 Pa. Rest of the parameters used were as per (Li, 2023).

S.no.	Parameter	Value
1.	Mass density	2660
2.	Elastic shear modulus (Pa)	20.28

3.	Eroding Plastic Strain	2.0
4.	Parameter for polynomial EOS, Bo	1.22
5.	Parameter for polynomial EOS, B1	1.22
6.	Parameter for polynomial EOS, T1 (Pa)	51.57e9
7.	Parameter for polynomial EOS, T2 (Pa)	0.0
8.	Failure surface parameter, A	2.57
9.	Failure surface parameter, N	0.75
10.	Compressive strength (Pa)	259e6
11.	Crush pressure PEL (Pa)	172.67e6
12.	Relative shear strength	0.21
13.	Relative tensile strength	0.10
14.	Load angle dependence factor, Qo	0.68
15.	Load angle dependence factor, B	0.05
16.	Reference compressive strain EOS (S-1)	3e-5
17.	Reference tensile strain rate ETC (S-1)	3e-6
18.	Break compressive strain rate EC (S-1)	3e25
19.	Break tensile strain ET (S-1)	3e25
20.	Compressive strain rate dependence exponent	0.026
21.	Tensile strain rate dependence exponent	0.007
22.	Volumetric plastic strain fraction in tension	0.001
23.	Compressive yield surface parameter	0.53
24.	Tensile yield surface parameter	0.70
25.	Shear modulus reduction factor	0.50

26.	Damage parameter, D1	0.04
27.	Damage parameter, D2	1.00
28.	Minimum damaged residual strain	0.015
29.	Residual surface parameter	1.60
30.	Residual surface parameter, NF	0.61
31.	Gruneisen gamma, GAMMA	0.0
32.	Hugonoit polynomial coefficient, A1 (Pa)	51.57e9
33.	Hugonoit polynomial coefficient, A2 (Pa)	60.23e9
34.	Hugonoit polynomial coefficient, A3 (Pa)	9.76e9
35.	Compaction pressure, PCO (Pa)	6e9
36.	Porosity exponent NP	3.0
37	Initial porosity	1.006

Table 2 Properties of Barre Granite, RHT Model from (Li, 2023)

Explosive:

Mat_High_Explosive Burn along with the Jones Wilkins Lee, Equation of State is used as per (Wang, 2018). The explosive used in the blasting operation is modeled by MAT_HIGH_EXPLOSIVE_BURN in LS DYNA (Material type 008) together with Jones- Wilkins-Lee EOS (LSTC, 2007)is used to describe the explosive as it is the most popular one and the easiest to calibrate. The EOS defines the pressure as follows:

$$P = A\left(1 - \frac{\omega}{R_1 V}\right)e^{-R_1 V} + B\left(1 - \frac{\omega}{R_2 V}\right)e^{-R_1 V} + \frac{\omega E}{V}$$

In the above equation V is the relative volume or the expansion of the explosive, E is the initial energy per volume, v_D is the detonation velocity, P_{CJ} is the pressure at the critical point, A, B, R_1, R_2 and ω are the empirically derived constants for the explosives. This equation allows the use of a wide range of different high explosive parameters such as TNT.

The parameter according to (Banadaki, 2010):

Parameters	DYNO Cord (PETN)
ρ (kg/m^3)	1630
Velocity of Detonation (VOD)	6690
P_{CJ}(GPa)	1.6e10
A (Pa)	5.86e11
B (Pa)	2.16e10
R_1	5.81
R_2	1.77
ω	0.282
V	1
E0 (J/m^3	7.38e9

Table 3 Properties of DYNO Cord Explosive as per (Banadaki, 2010)

Air Model:

The air is represented using an ideal gas model employing the MAT_NULL material model, which incorporates a linear polynomial Equation of State (EOS). The use of the null material model proves effective in accurately simulating fluids and hydrodynamic substances. The pressure is expressed by:

$$P = C_0 + C_1\mu + C_2\mu^2 + C_3\mu^3 + (C_4 + C_5\mu + C_6\mu^2)E$$

Where,

E= internal energy per unit volume

$C_0, C_1, C_2, C_3, C_4, C_5$ and C_6 = constants

$\mu = \frac{\rho}{\rho_0} - 1$, where $\frac{\rho}{\rho_0}$ is the ratio of current density to initial density.

The linear polynomial equation represents an ideal gal with the gamma law EOS, in which $C_0 = C_1 = C_2 = C_3 = C_6 = 0$ and $C_4 = C_5 = \gamma - 1$

where, γ is the ratio of specific heat at constant pressure per specified heat at constant volume.

The pressure is then described by:

$$P = (\gamma - 1)\frac{\rho}{\rho_0}E_0$$

$$E_0 = \rho_0 c_v * T$$

γ is an adiabatic constant for air behaving as an ideal gas, ρ is the density, c_v is the specific heat at constant volume and E_0 is the initial internal energy per unit volume.

The material parameters according to Wang (2018) is as follows:

Parameter	Details
Density (kg/m3)	1.29
PC	0
C0	0
C1	0
C2	0
C3	0
C4	0.4
C5	0.4
C6	0
Eo(Pa)	2.5e5
Vo	1

Table 4 Properties of Air

Copper Model:

The Johnson-Cook Model, a metal constitutive model, was employed to characterize the copper material, and it is entirely empirical in nature. The parameters for Johnson Cook Model, (Wang, 2018)is as follows:

S.No.	Parameter	Detail
1.	Density (kg/m3)	8330
2.	Young's Modulus (Pa)	1.38e10
3.	Poisson's ratio	0.35
4.	A (Pa)	8.963e7
5.	B (Pa)	2.916 e8
6.	N	0.31
7.	C	0.025
8.	M	1.09
9.	Melting Temperature	1200
10.	Room Temperature	30
11.	Specific Heat	4400
12.	C (Gruneisen EOS)	0.394

13.	S1	1.489
14.	S2	0
15.	S3	0
16.	Gamma	2.02
17.	A (Gruneisen EOS)	0.47
18.	Eo	0

Table 5 Properties of Copper, Johnson Cook Model as per (Wang, 2018)

Polyethylene model:

Polyethylene was modeled with Mat_Null with Equation of state, EOS_Gruneisen.

The parameters for polyethylene (Wang, 2018) are as follows:

S.No.	Parameter	Details
1.	Density (kg/m3)	79
2.	Bulk sound Speed (m/s)	290.1
3.	Material constant, S1	1.481
4.	Material constant, S2	0
5.	Material constant, S3	0

Table 6 Properties of Polyethylene

Results of the Study:

The numerical results depict the presence of cracks through the utilization of damage contours that span from 0 to 1. Blue signifies fringe level 0, indicating the absence of damage to the rock, while red signifies fringe level 1, indicating complete damage in the rock. In essence, the red contour denotes the area of crushing, while the green contour represents the circumferential and radial cracks. The remaining colors, which correspond to fringe levels 0 and 1, signify varying degrees of damage in the rocks.

Figures 8 to 15 illustrate a close alignment between the outcomes of our 3D model and those derived from the experiment. The simulation shows the generation of crush zones near the blast holes, accompanied by radial cracks extending towards the outer boundaries upon detonation. The scale of damage decreases gradually as one moves away from the blast hole. Near the blast hole, the damage exhibits a dispersed crossing pattern, whereas in the farther zone, it takes on a radial pattern, ultimately

leading to the creation of a fractured zone.

The cracking in the bottom of the model is more than that in the top because the explosive is detonated at the bottom. This is very similar to the (Banadaki, 2010) experiment.

Both the JH-2 model and RHT model are successful in predicting the pattern of cracks. However, the RHT model generated more crushed zone indicated by red area compared to the JH-2 model. Similarly, the number of radial cracks were more for RHT model compared to the JH-2 model. However, the circumferential cracks were generated by the JH-2 model but not generated by the RHT model.

The close similarity between the experimental results and the numerical simulation proves that both the JH-2 model and RHT model can be used for simulating the explosion process of rocks, provided that the parameters are carefully calibrated. The thesis will now be focused on exploring the effects of decoupling ratio on the blast damage as well as the effects of spacing of blastholes on the damage of rocks. **RHT model is preferred over JH-2 model due to close similarity in the cracking and the damage pattern.**

Description	Crushed zone diameter	Radial Cracks	Circumferential Cracks
JH-2 model	16mm	8	More
RHT model	16mm	14	Few

Table 7 Comparison between the JH-2 model and RHT Model

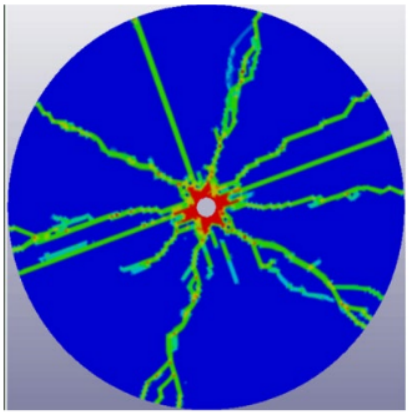

Figure 8 Damage Pattern in in the top of the numerical model, (Wang, 2018)

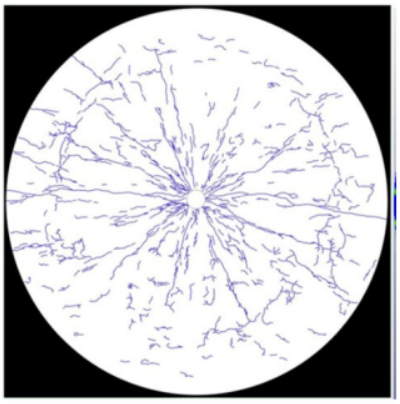

Figure 9 Result of the (Banadaki, 2010) experiment in the top

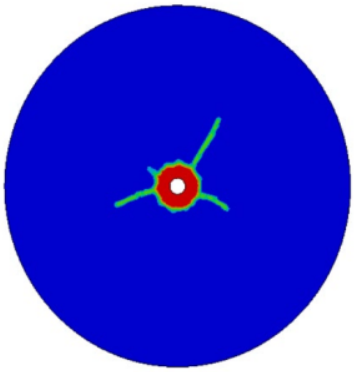

Figure 10 Damage pattern at the top with JH-2 model

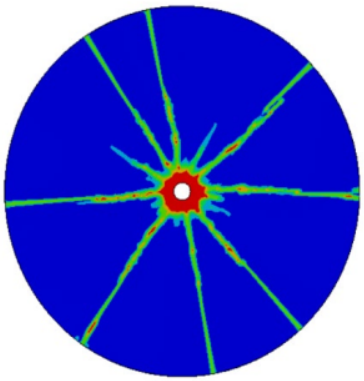

Figure 11 Damage pattern at the top with RHT model

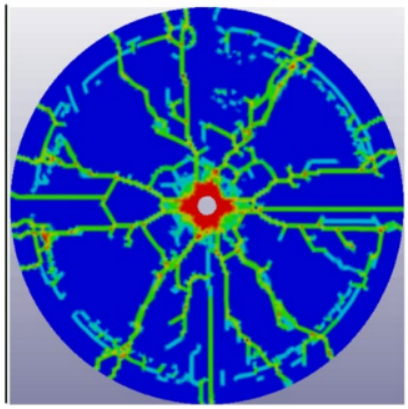

Figure 12 Damage pattern in the top of the model , (Wang, 2018)

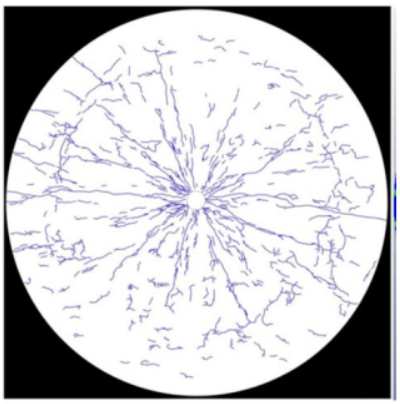

Figure 13 Crack pattern in the bottom of the sample, (Banadaki, 2010)

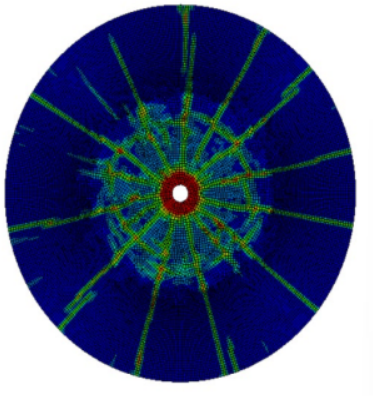

Figure 14 Result of damage pattern in the sample from RHT model

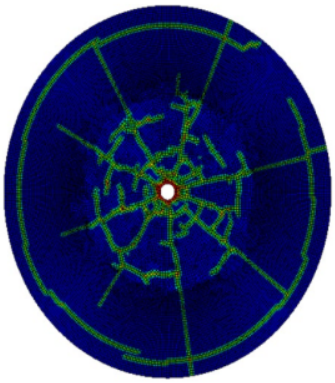

Figure 15 Result of the damage pattern in the bottom of the model from JH-2 model

4. INFLUENCE OF DECOUPLING RATIO ON BLASTING IN BARRE GRANITE

4.1 Background and Literature Review:

In blasting practices, air and water have been employed as coupling media, with the efficacy of the blasting process contingent on various factors. These factors encompass rock properties, hole diameter, charge length, stemming material type, initiation point, and decoupling. The decoupling factor, defined as the ratio of the drill hole radius to the charge radius (Ucar, 1975), holds significance, particularly in smooth blasting and presplitting blasting applications.

Controlled blasting, aimed at reducing peak pressure and optimizing blasting energy utilization, relies on proper decoupling. Notably, when the explosive charge doesn't completely fill the hole, the imparted energy diminishes significantly. Research by (Wang W. L., 2020) demonstrated the pivotal role of the uncoupling coefficient in blasting-induced damage. (Ding, 2021) concluded that judicious decoupling enhances crack propagation and soil fragmentation. (Ma, 2022), utilizing ANSYS AUTODYN software, observed a substantial alteration in blasting damage up to a decoupling coefficient of 3. (Song, 2019) determined that the optimal blasting effect occurs within a decoupling coefficient range of 1.67-2.

Additionally, (Yang, 2018) found that stress attenuation initially increases and then decreases with an increase in the decoupling coefficient. (Li, 2023) delved into the effects of air-water ratio and decoupling ratio on rock fragmentation, shedding further light on the intricate dynamics of decoupling in blasting scenarios.

4.2 Details of Numerical Model:

Two different numerical models are established to investigate the effects of decoupling ratio on the damage and crack propagation. The rock material is Barre Granite as in Chapter 1. RHT constitutive model is used for the rock and High Explosive burn along with Jones Wilkins Lee Equation of State is used for modeling the PETN explosive. The air is modeled using MAT_Null and Equation of State Linear Polynomial. Five numerical models have been created with decoupling ratio, k=1, k=1.5, k=2.5, k=3 and k=4 to understand the damage patterns induced by the changing decoupling ratio with air as decoupling media. Furthermore, in the same

numerical model, further analysis was done by substituting water as the decoupling media and comparisons made between the both.

The dimension of the numerical model is 2m x 2m x 1m. A blasthole of 45 mm has been used for all the experiments. For the decoupling ratio, k=1, k=1.5, k=2.5,k=3 and k=4, the drillhole diameters are 45mm, 67.5 mm, 112.5mm , 135 mm and 180 mm respectively. The mesh size used was 2.5 cm x 2.5 cm x 10 cm. Lagrangian formulation is used to model the rock. ALE formulation is used to model the air and TNT. Constrained_Lagrange_in_Solid is used for Fluid Structure Coupling between rock and air and explosive. Nodes were merged at the interface. The explosives were detonated at the top. Nonreflecting boundary condition were applied at the boundaries except the top to simulate the infinite rock medium. The explosive was detonated from the top. The purple color indicates explosive whereas the green and red color indicate air and the rock respectively.

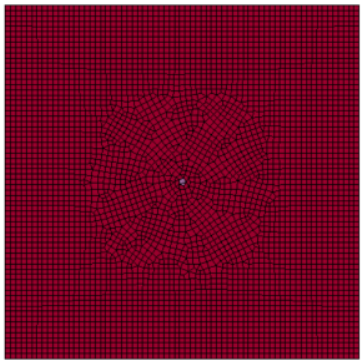

Figure 16 Detail of numerical model, k= 1.

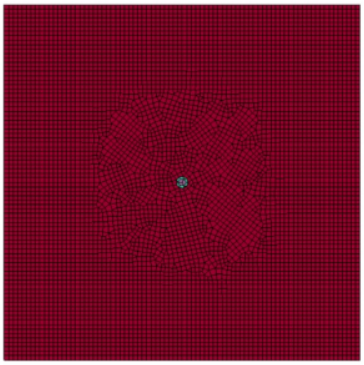

Figure 17 Detail of numerical model, k= 1.5

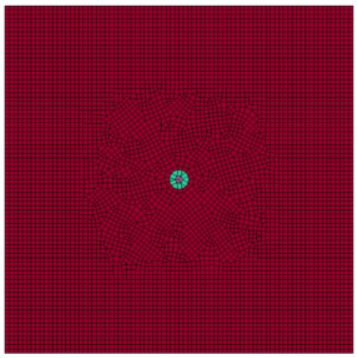

Figure 18 Detail of numerical model, k= 2.5

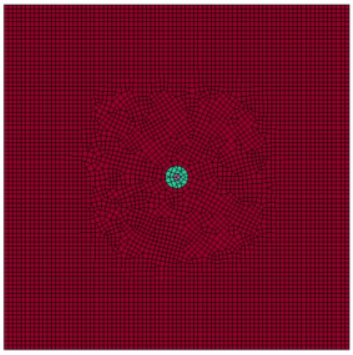

Figure 19 Detail of numerical model, k= 3

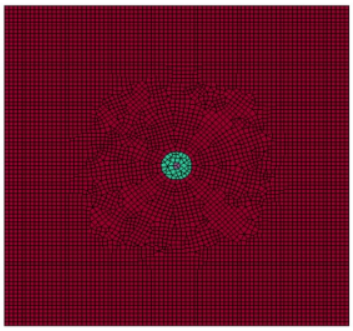

Figure 20 Detail of numerical model, k= 4

4.3 Material Parameters

The material parameters were the same as that used in the (Banadaki, 2010) experiment on Barre Granite. RHT material was used for modeling the rock. The parameters for the rock, air and explosive are the same as in Table 2, Table 3 and Table 4. For water, the parameters are as follows:

4.4 Results with air as decoupling media

For the decoupling ratio of 1, the damage pattern is as shown in Figure 22. The crushed zone indicated by the red zone has a diameter of around 0.4m with around 8 radial cracks shown by the green line.

For the decoupling ratio of 1.5, the damage pattern is as shown in Figure 23. The crushed zone has a diameter of around 0.36m with the number of radial cracks reduced to 6.

For the decoupling ratio of 2.5 (Figure 24), the crushed zone diameter is 0.25m and the radial cracks has reduced to 5.

For the decoupling ratio of 3 (Figure 25), the crushed zone diameter is 0.22m and the radial cracks are very few.

For the decoupling ratio of 4 (Figure 26), the crushed zone has diminished to 0.15m and radial cracks cannot be seen.

The damaged area for all five cases can be seen in Figure 21 and Table 8. For the analysis of the damaged area, the toral undamaged area calculated by image software (ImageJ) is used. To obtain the undamaged area, the damaged area shown by the colors except blue are calculated. The area is deducted by 100 to obtain the percentage of damaged area.

Decoupling coefficient	Damaged Area(%)
1	18.72
2	15.49
3	4.15
4	3.95
5	1.46

Table 8 Relation between Decoupling Coefficient and Damaged Area

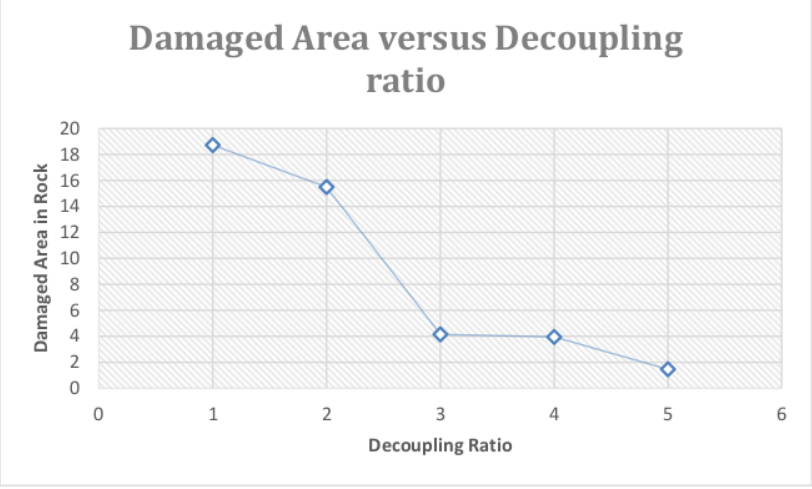

Figure 21 Influence of Decoupling ratio on Damaged Area

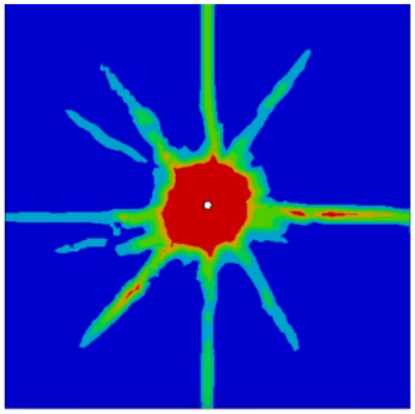

Figure 22 Damage pattern for decoupling ratio of 1

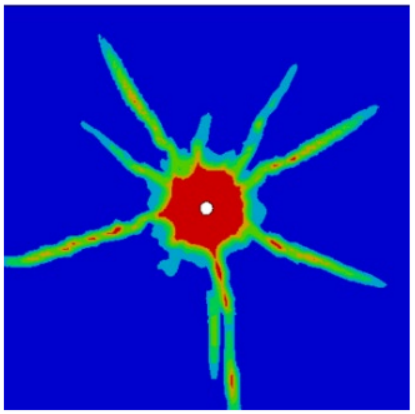

Figure 23 Damage pattern for decoupling ratio of 1.5

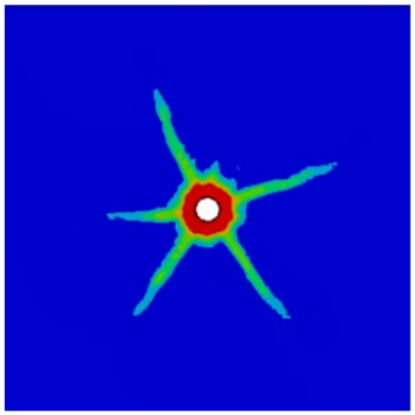

Figure 24 Damage pattern for decoupling ratio of 2.5

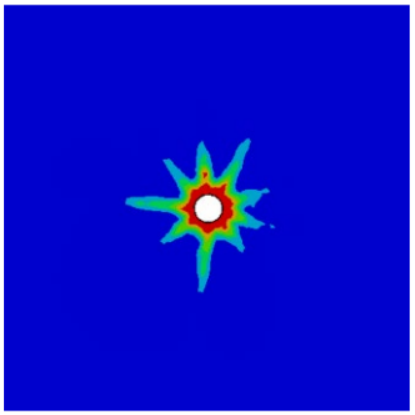

Figure 25 Damage pattern for decoupling ratio of 3

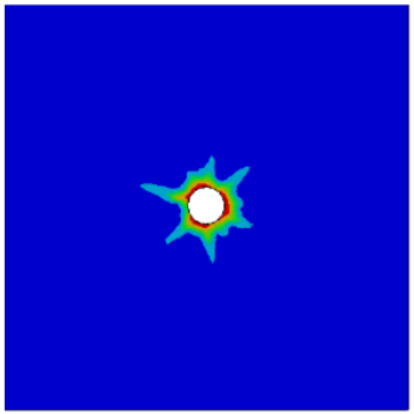

Figure 26 Damage pattern for decoupling ratio of 4

Similarly, the blasting pressure provides a quantitative glimpse into the mecahnism of wave pressure attenuation due to the decoupling coefficients. To obtain the pressure distribution, the blasthole wall pressures are obtained and plotted. Figure 27 to 29 show the Blasthole wall pressure for the Decoupling coefficient of 1, 1.5,2.5,3 and 5.

The pressure for blasthole for decoupling coefficient are shown in the Figures 27 to 31. Figure 27 shows the peak blasthole pressure for k=1 which is 3000 MPa. Figure 28 shows the peak presure for k=1.5 which is 1000 Mpa. The borehole pressure decreased highly for k=2.5 to 400 Mpa, which can be seen in Fig.29. The pressure slightly decreased for k=3 to 250 Mpa, shown in Fig.30. However, there is a slight increase in pressure for k=4 to 200 Mpa, shown in Fig. 31.

The blasthole wall pressure provides a good indication of the blastwave pressure induced to the rock. As shown in the above figures, it can be clearly seen that when there is no air,i.e. k=1, very high blastwave pressure is transmitted to the rock. For k=1.5, the pressure is still very high. However, as the value of k increased to 2.5, there was almost a drop of pressure to 4 times. Then, for k=3.5, there was slight decrease in pressure. For k=4, there was a further decrease in pressure.

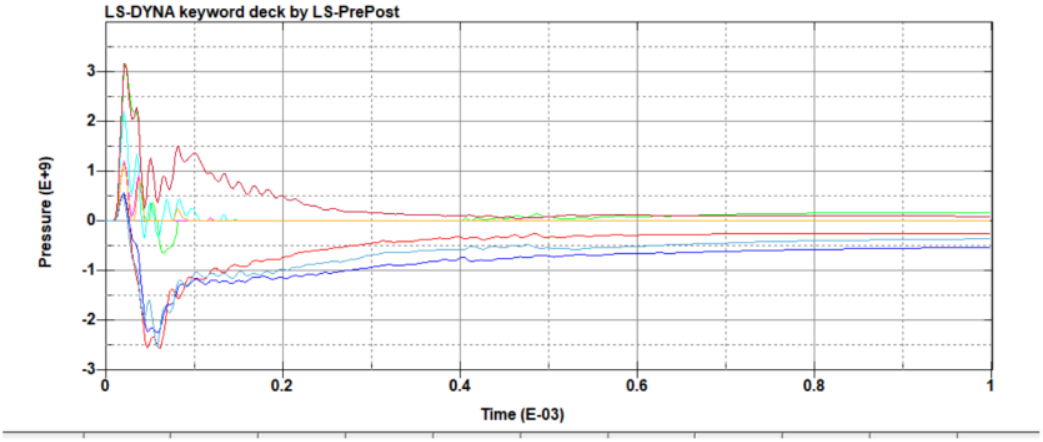

Figure 27 Borehole wall pressure for decoupling ratio of 1

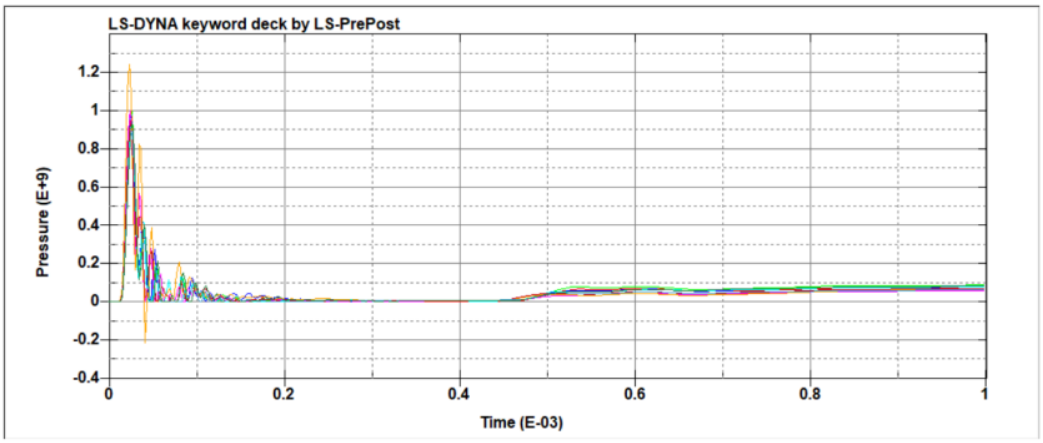

Figure 28 Borehole wall pressure for decoupling ratio of 1.5

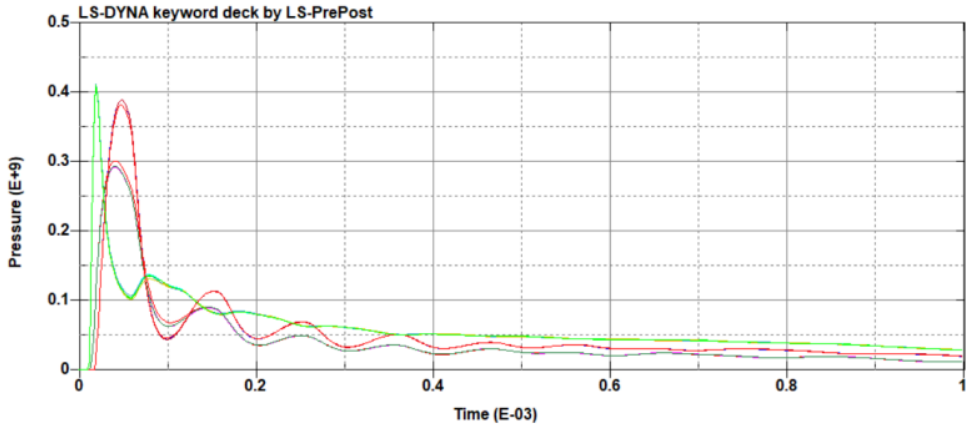

Figure 29 Borehole wall pressure for decoupling ratio of 2.5

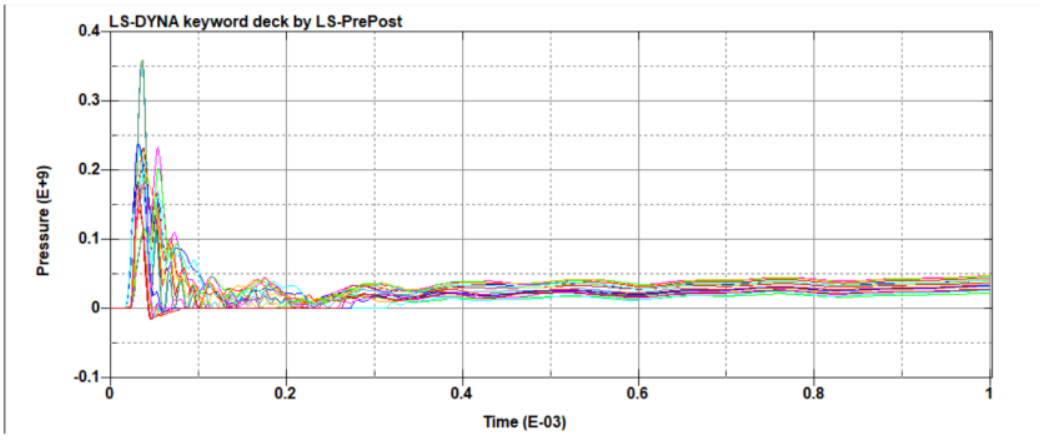

Figure 30 Borehole wall pressure for decoupling ratio of 3

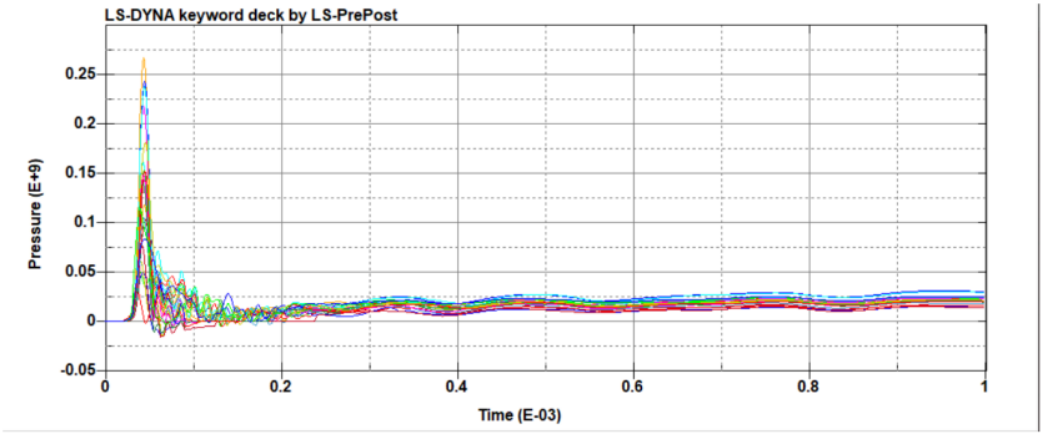

Figure 31 Borehole wall pressure for decoupling ratio of 4

S.no.	Decoupling coefficient	Pressure
1	1	3000
2	1.25	1000
3	1.5	1000
4	1.75	600
6	2.5	400
7	3	250
8	4	200
9	5	30

Table 9 Pressure for Different Decoupling Coefficient, Air as Decoupling Media.

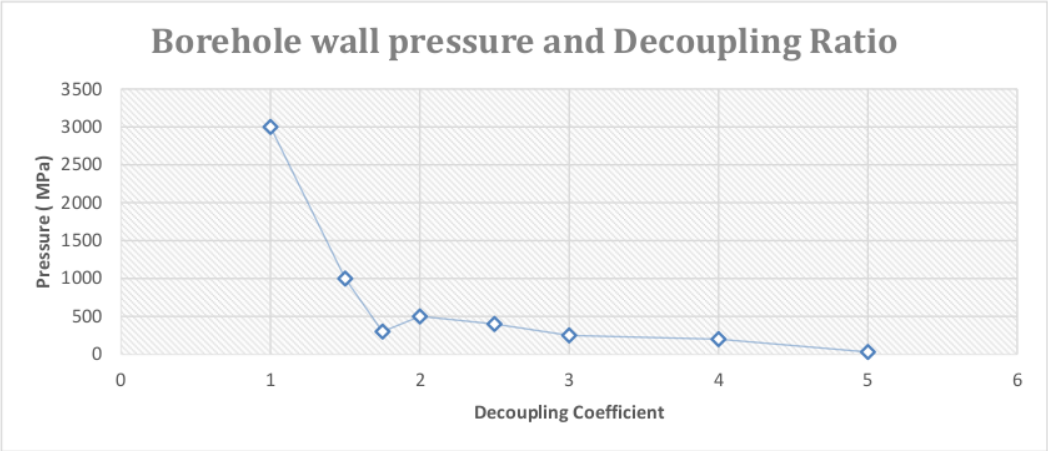

Figure 32 Peak Pressure in Blasthole for different Decoupling ratios

It can be seen from the above figures that as the decoupling ratios increases, the blasthole pressure decreases. However, when the decoupling ratio exceeds 2, the blasthole pressure stays nearly the same. Therefore, it can be concluded that as decoupling ratio increases, initially there is a drastic reduction in damage of the rocks. However, with further increase in the ratio, the damage to the rocks progressively becomes insignificant.

4.5 Results of Comparison between air and water as decoupling Media

The numerical simulation was conducted with water as the decoupling media instead of the air and the blasthole pressures were noted in the same locations as before. The distribution of Pressure with time is shown in the following figures.

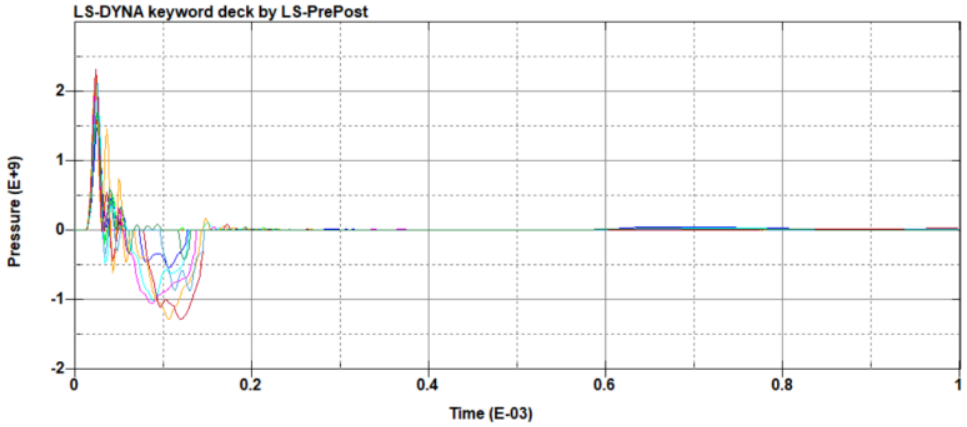

Figure 33 Blasthole Pressure for Water Decoupling, k=1.5

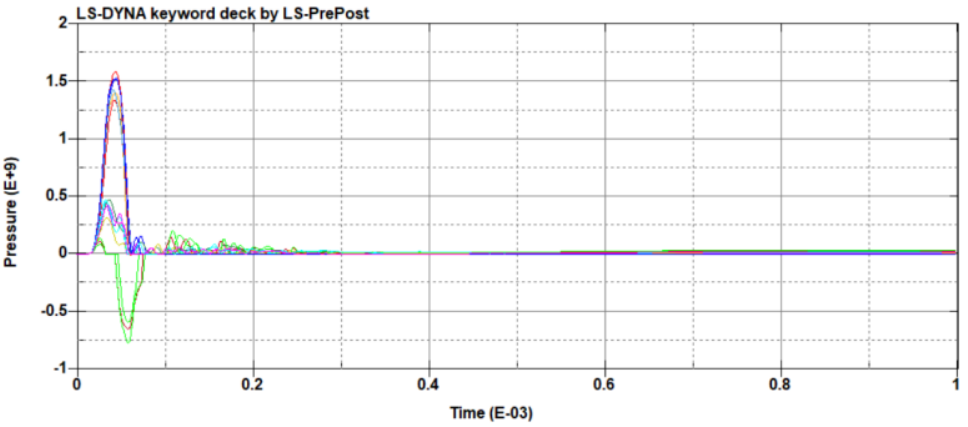

Figure 34 Blasthole Pressure for Water Decoupling, k=2.5

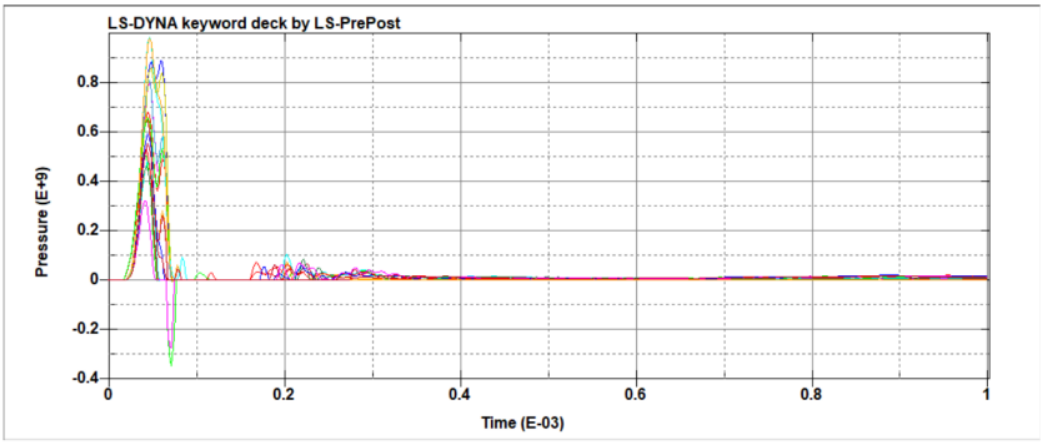

Figure 35 Blasthole Pressure for Water Decoupling, k=3

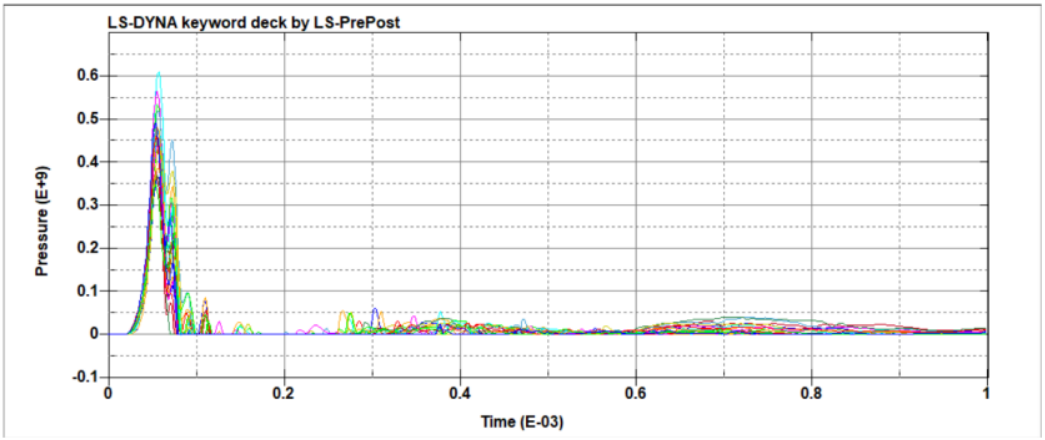

Figure 36 Blasthole Pressure for Water Decoupling, k=4

S.No.	Decoupling Coefficient	Blasthole Pressure (MPa)	
		Air	Water
1.	1	3000	3000
2.	1.5	1000	2000
3.	2	500	1500
4.	3	250	850
5.	4	200	550

Table 10 Decoupling ratio and Pressure for Different Coupling Media

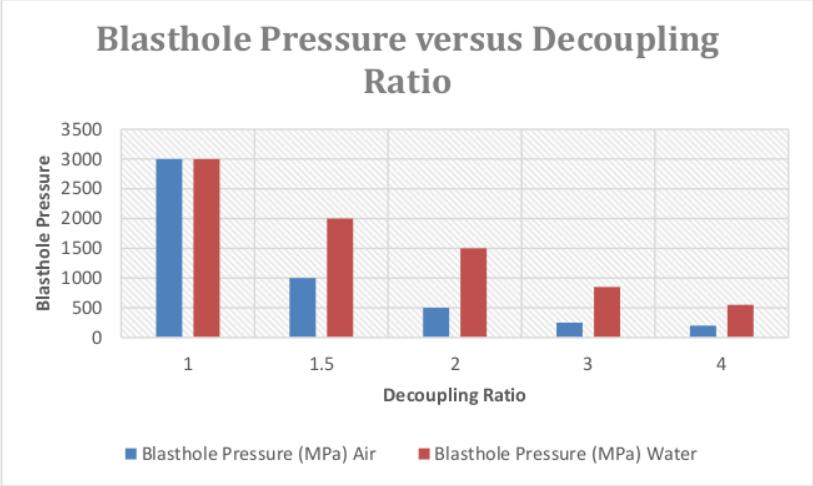

Table 11 Influence of Decoupling ratio on Blasthole pressure for Different Decoupling Media

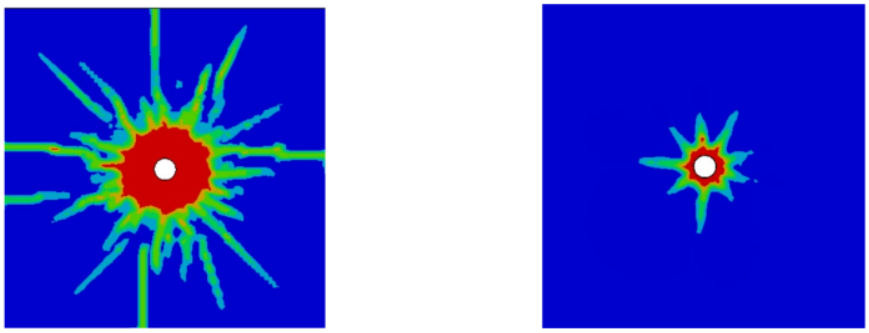

Figure 37 Damage contour for Water and Air Decoupling, k=2.5

Therefore, it can be observed that compared to air, more pressure is transferred by the water as the coupling media. The pressure readings obtained for water decoupling are considerably high compared to the air media. Similarly, from the damage contours obtained, there is considerably low damage with air than in the water as can be seen with more blue area with air compared to water. Therefore, about energy dissipation, air is a better decoupling medium. Similarly, the pattern of pressure dissipation with the decoupling ratio for both the decoupling media is similar. Both the media showed drastic reduction in pressure dissipation at the lower decoupling ratio but with the increase in the ratio there is a lesser reduction of pressure. In this way, the influence of decoupling ratio on blast induced damage was investigated.

5. EFFECT OF DELAY TIME OF EXPLOSION AND BOREHOLE SPACING ON BLAST INDUCED ROCK DAMAGE

The effect of blasthole spacing on crack propagation and damage of the rocks is analyzed in this section. A numerical model is established in the same principle to the decoupling experiment.

5.1 Geometry of the Model

A numerical model is created with the dimensions of 2m x 2m x 1m. Two blastholes are created with diameter of 45mm each. For the first case, two spacings of blastholes, 0.4m and 0.5m are used. Various Delay times are used, and the damage subsequently induced are analyzed. For the second case, various spacings are created to analyze the effect of spacing blasting. A total of six models are created with the spacings between the blastholes of 0.1m, 0.2m, 0.3m, 0.4m, 0.5m and 0.6m. PETN explosive is used in the blasthole. The decoupling coefficient is kept as 1. The explosive is detonated from the top.

The rock is modelled as Lagrange elements and the explosive, PETN and the air is modelled as ALE elements. Constrained_Lagrange_in_Solid is used for Fluid Structure Coupling. ALE Multi Material Group is created separately for the air and explosive. The nodes are merged at the interface of the elements. Nonreflecting boundary condition is used to simulate the infinite medium. The model is run for a time period of 1 x 10-4 seconds.

5.2 Material Parameters

RHT constitutive model is used to model the Barre Granite sample as per Table 2. MAT_HIGH_EXPLOSIVE_BURN and EOS_JWL is used for the explosives as per Table 3. STRFLG is set as 4 in DATABASE_BINARY_EXTENT for providing the damage plots for the rock.

5.3 Influence of Delay time on Blast Induced Damage:

The primary aim in optimizing rock fragmentation is to minimize energy consumption. Substantial research undertaken by scholars and engineers has focused on improving rock blasting methodologies to achieve superior fragmentation, constituting a longstanding area of study. Among the critical factors explored in these investigations, the timing of blasts emerges as a pivotal variable. Given the dynamic

nature of blast phenomena, it becomes evident that stress waves originating from different blastholes will inevitably interact within the rock mass.

A fundamental question arises concerning the consequences of this interaction on both fragmentation and damage in the rock mass. While existing studies have suggested that a concise delay time may contribute to heightened fragmentation, a precise understanding of the extent of damage resulting from varying delay times remains elusive. This underscores the need for further research to unravel the intricate dynamics of blast timing and its impact on rock fragmentation and damage.

Attempt has been made to understand the effects of delay time on the blast induced damage. For the purpose, the numerical model as shown above is used. Two cases have been explored. In the first case, the borehole spacing is taken as 0.4m and in the second case the borehole spacing is taken as 0.5m. The results are as follows:

S.No.	Delay time (seconds)	Crushed Area (%)
1	0	8.81
2	0.0000001	8.78
3	0.0000005	8.78
4	0.000001	8.76
5	0.000005	8.81
6	0.00001	8.77
7	0.00002	8.85
8	0.00003	9.28
9	0.00004	9.29
10	0.00005	9.56
11	0.00006	9.22
12	7.00E-05	9.21
13	8.00E-05	9.3
14	9.00E-05	9.57
15	0.0001	9.39
16	0.000125	9.76
17	0.00015	10.12
18	0.00025	10.68
19	5.00E-04	10.76
20	0.00075	10.55
21	1.00E-03	10.64
22	0.00150	10.51
23	2.00E-03	10.34
24	3.00E-03	10.18
25	5.00E-03	9.66
26	1.00E-02	9.48
27	2.00E-02	9.3

28	5.00E-02	9.3

Table 12 Influence of Delay time of explosives in crushed area of rocks, for blasthole spacing of 0.4m

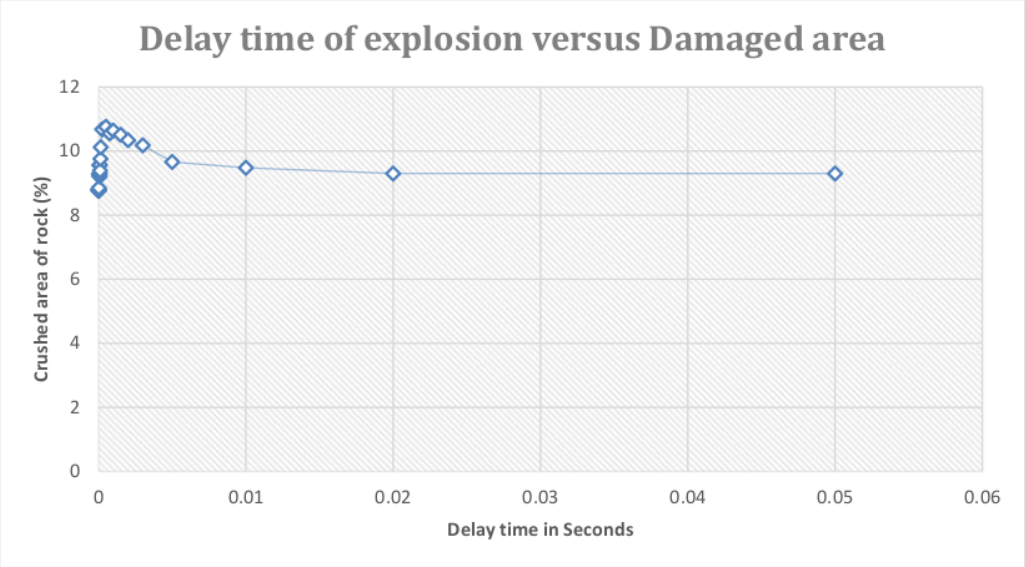

Table 13 Influence of Delay time of explosion to the damage in the rocks, for borehole spacing of 0.4m

S.No.	Delay Time (seconds)	Crushed Area
1	0	9.1
2	0.0000001	9.08
3	0.0000005	9.42
4	0.000001	9.03
5	0.000005	9.17
8	0.00001	9.27
9	0.00002	9.19
11	0.00004	9.49
12	0.00005	9.72
13	0.00006	9.78
14	7.00E-05	9.63
16	9.00E-05	10.12
17	0.0001	10.22
20	0.00025	10.61
21	5.00E-04	11.65
22	0.00075	11.63
23	1.00E-03	12.08
24	0.00150	11.92

25	1.75E-03	11.68
26	3.00E-03	11.44
27	5.00E-03	11.25
28	7.00E-03	11.26
29	2.00E-02	11.06
30	5.00E-02	10.82
31	7.50E-02	10.7

Table 14 Influence of Delay time of explosives in crushed area of rocks, for blasthole spacing of 0.5m

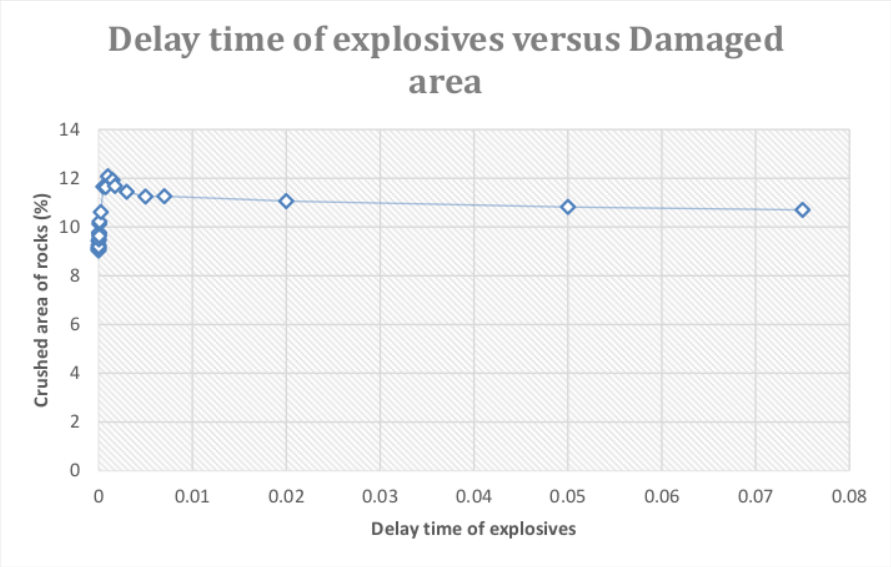

Table 15 Influence of Delay time of explosives to the Damage in the rocks, for blasthole spacing of 0.5m

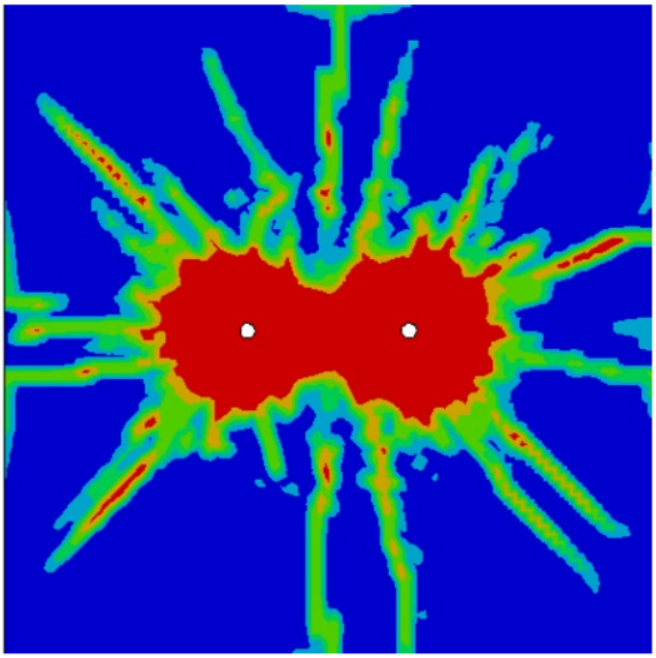

Figure 38 Blast induced damage for 0 delay time between detonation of explosives

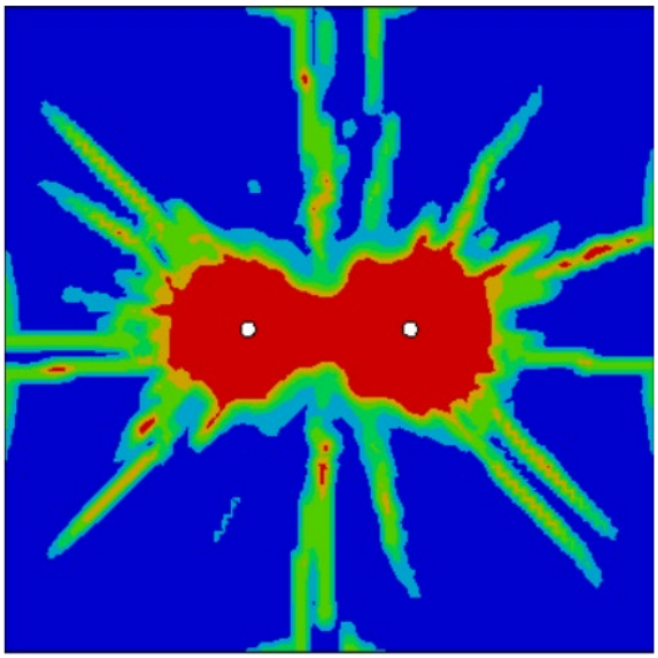

Figure 39 Blast damage for 1e-6 delay time between detonation of explosives.

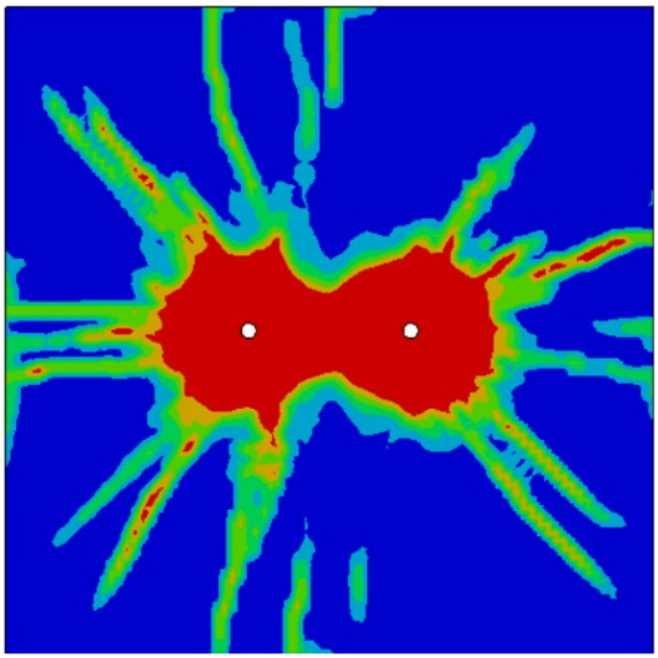

Figure 40 Blast induced damage for 5e-5 delay time between the detonation of explosives.

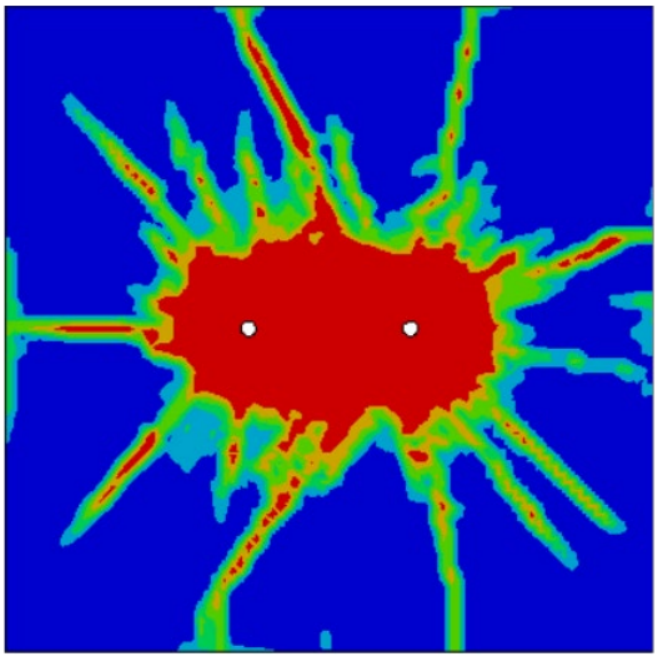

Figure 41 Blast induced damage for 5e-4 seconds delay time between the detonation of explosives.

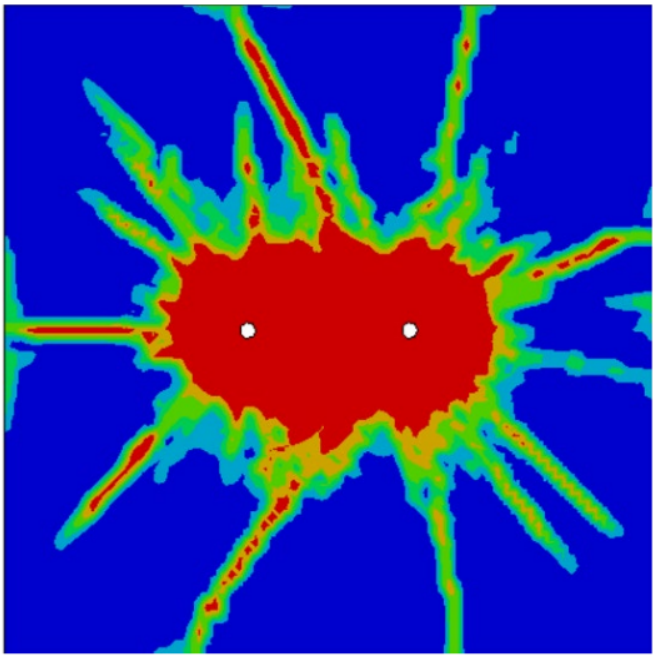

Figure 42 Blast induced damage for 1e-3 delay time between the detonation of explosives.

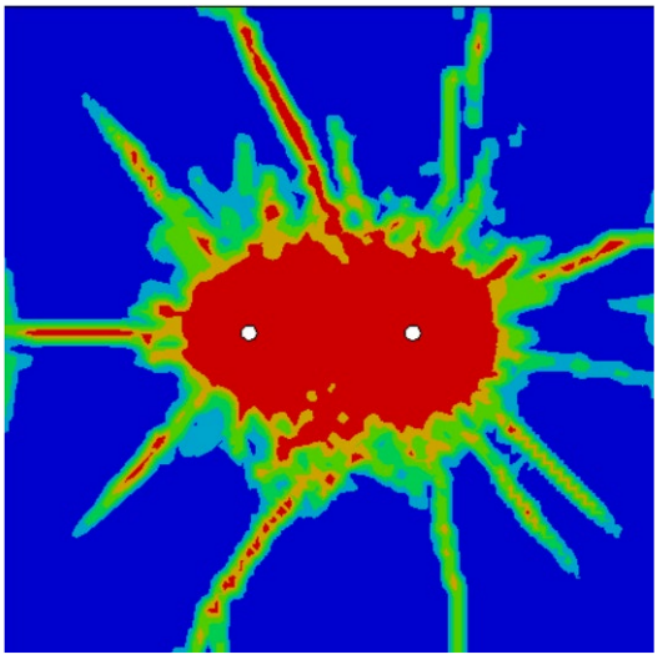

Figure 43 Blast induced damage for 1e-2 delay time between the detonation of explosives.

For both the cases of spacing of 0.4m and 0.5m, initially there is an increase in the total crushed area with the subsequent increase in the delay interval of the explosives. For 0.4m spacing, the simultaneous detonation of explosives produced a damage area

of 8.81%. The delay time was subsequently increased for the further simulations. It was found that up to the delay time of 2e-5 seconds, there was not much effect of the delay time on damage. When the delay time was 3e-5 seconds, the damage area slightly increased to 9.28%. The blast induced damage continued to increase with the delay time and subsequently peaked at 5e-4 seconds to 10.76%. Thereafter, the crushed area started to decrease with the increase in delay duration. For the delay duration of 5e-2 seconds, the crushed area was found to be 9.3%.

Therefore, for borehole spacing of 0.4m, the optimum delay time between the explosions was found to be 5e-4 seconds.

For the spacing between the boreholes of 0.5m, a similar trend was found. The crushed area for simultaneous detonation was 9.1%. Up to the delay time of 2e-5 seconds, the crushed area was relatively unchanged. For delay time of 4e-5 seconds, the crushed area increased to 9.49%. Thereafter, there was a subsequent rise in the crushed area with the increase in delay time. The damaged area continued to increase continuously up to the delay time of 1e-3 seconds. The crushed area was 12.08% at this stage. For further increase in the delay time, the crushed area showed a decreasing trend. For 7.5e-2 seconds, the crushed area was found to be 10.7%.

Therefore, for borehole spacing of 0.5m, the optimum delay time between the explosions was found to be 1e-3 seconds.

It can be concluded that there is an optimum delay time for different spacings of boreholes as shown by the increasing damage up to that delay time and decrement in crushed are beyond that delay time. Similarly, it was found that the increment in spacing between the explosives, the optimum delay time is more.

5.4 Influence of Spacing of Blastholes on Rock Damage:

The damage pattern for the rock for different spacings is shown below. Figures 44 to 49 show the damage pattern for blastholes with spacings in horizontal direction from 0.1m to 0.6m. Similarly, Figures 50 to 55 show the damage pattern for blastholes with spacings in vertical direction from 0.1m to 0.6m.The red color indicates the maximum damage which is the crushed zone. Blue color indicates the undamaged zone. Green color indicates the radial cracks. The damage variable 4 is used to provide graphical image of damage for the RHT model of the rock. Image analysis was done to understand the extent of the damage to the rocks. The area of blue undamaged portion is calculated to estimate the percentage of rock undamaged by the blast wave. The remaining area is calculated as the damaged portion. Furthermore, the red area is calculated as the crushed zone.

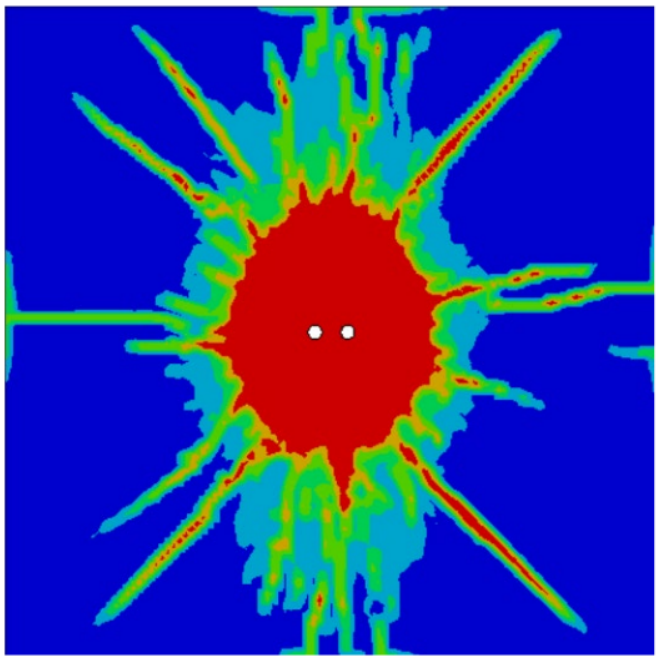

Figure 44 Damage pattern for horizontal blasthole spacing of 0.1m

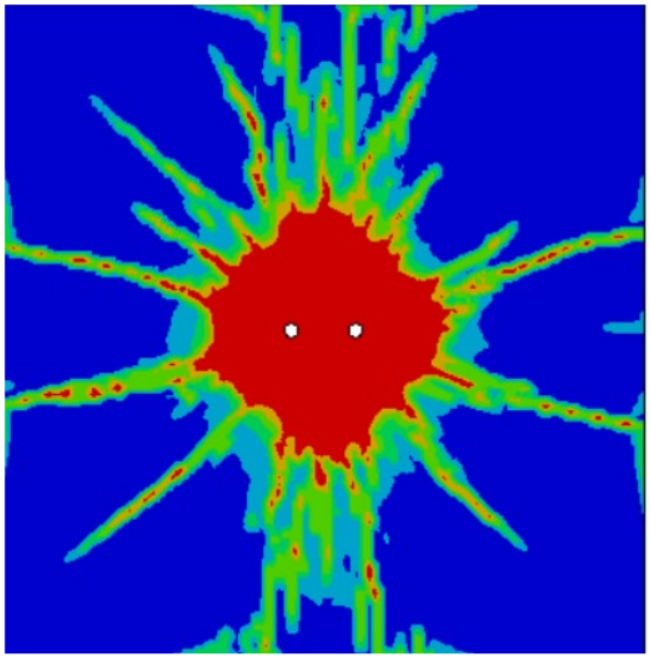

Figure 45 Damage pattern for horizontal blasthole spacing of 0.2m

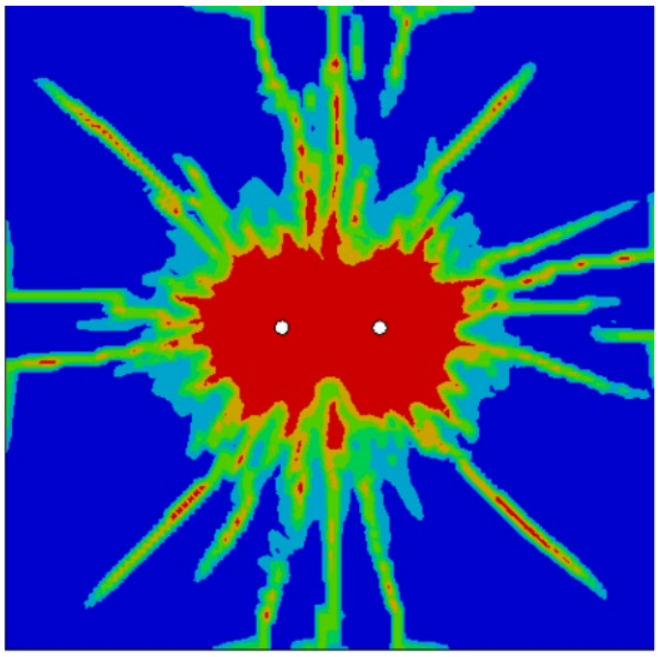

Figure 46 Damage pattern for horizontal blasthole spacing of 0.3m

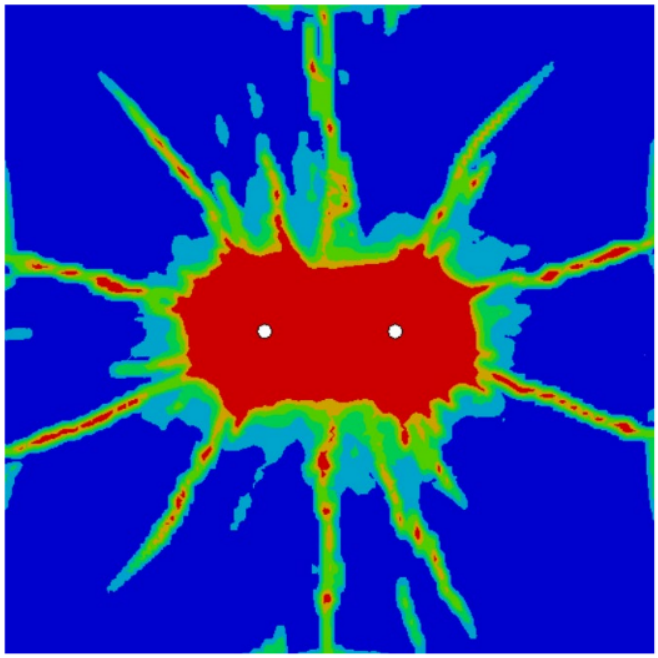

Figure 47 Damage pattern for horizontal blasthole spacing of 0.4m

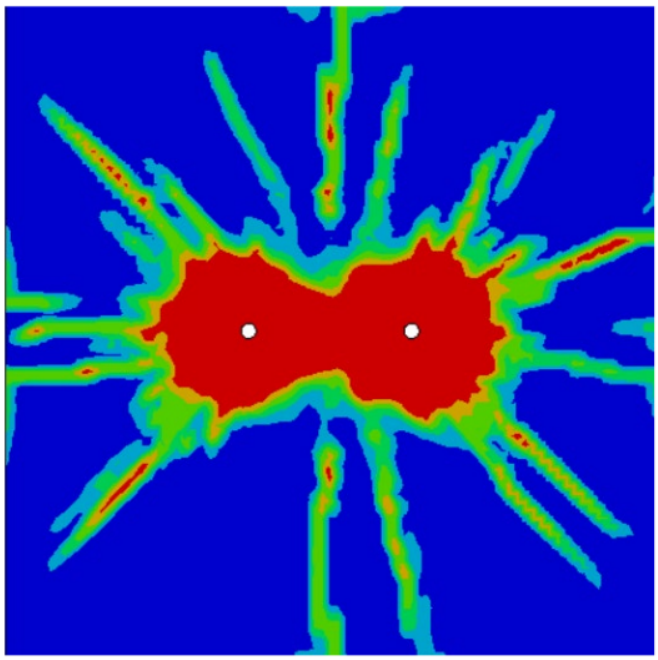

Figure 48 Damage pattern for horizontal blasthole spacing of 0.5m

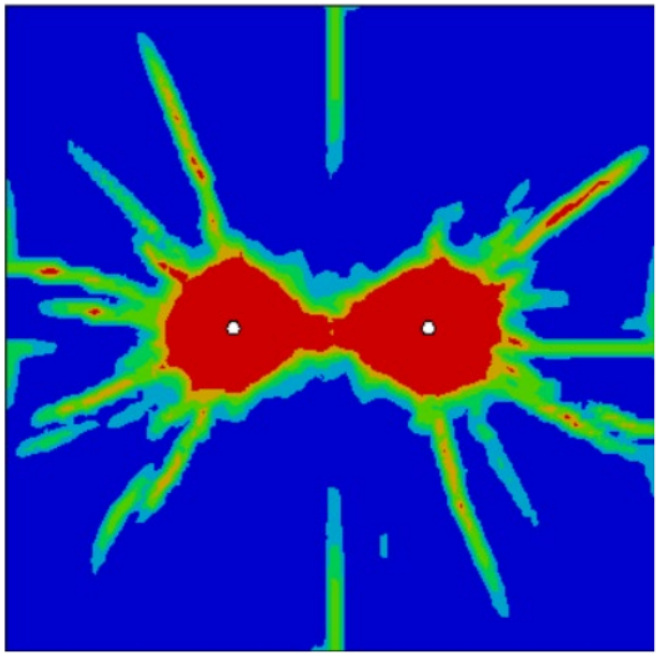

Figure 49 Damage pattern for horizontal blasthole spacing of 0.6m

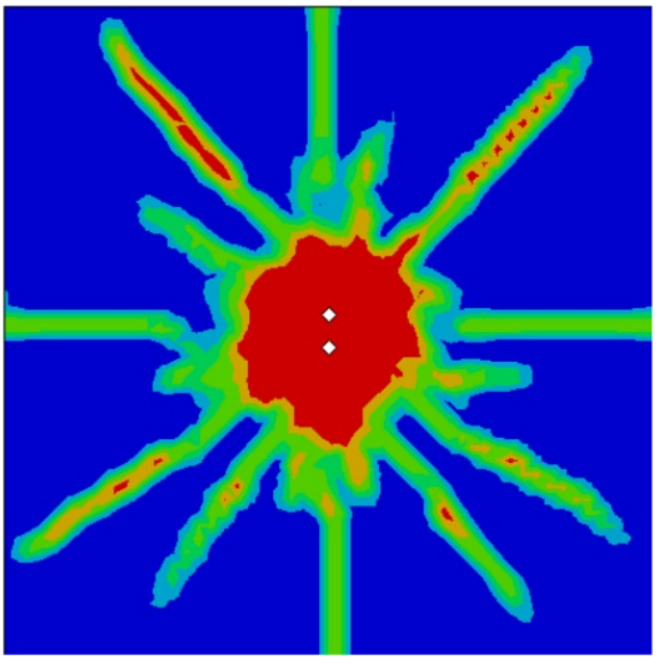

Figure 50 Damage pattern for vertical blasthole spacing of 0.1m

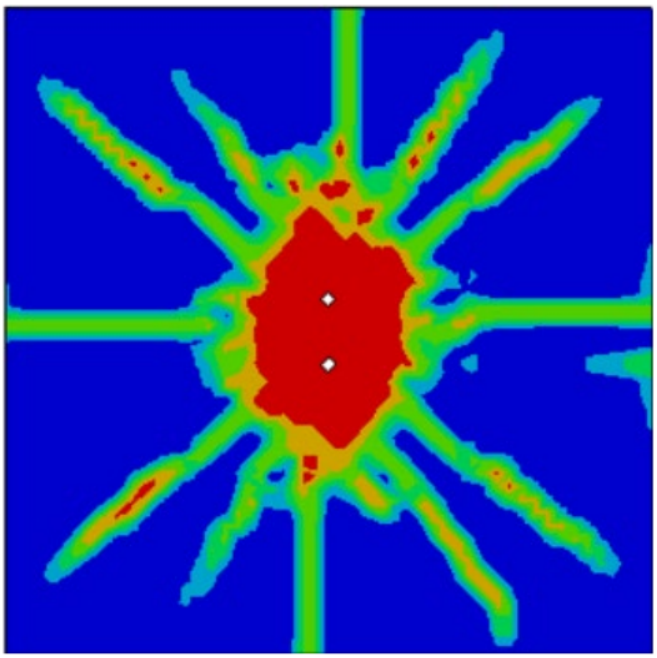

Figure 51 Damage Pattern for Vertical Blasthole Spacing of 0.2m

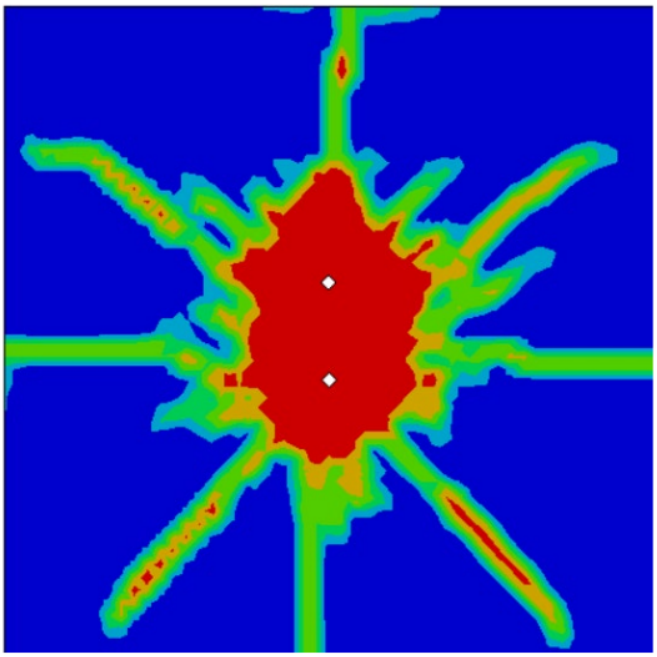

Figure 52 Damage Pattern for Vertical Blasthole Spacing of 0.3m

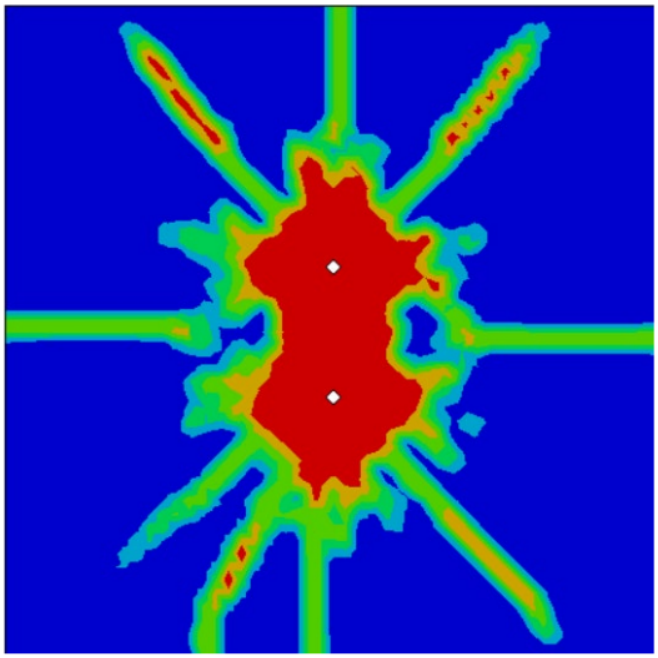

Figure 53 Damage Pattern for Vertical Blasthole Spacing of 0.4m

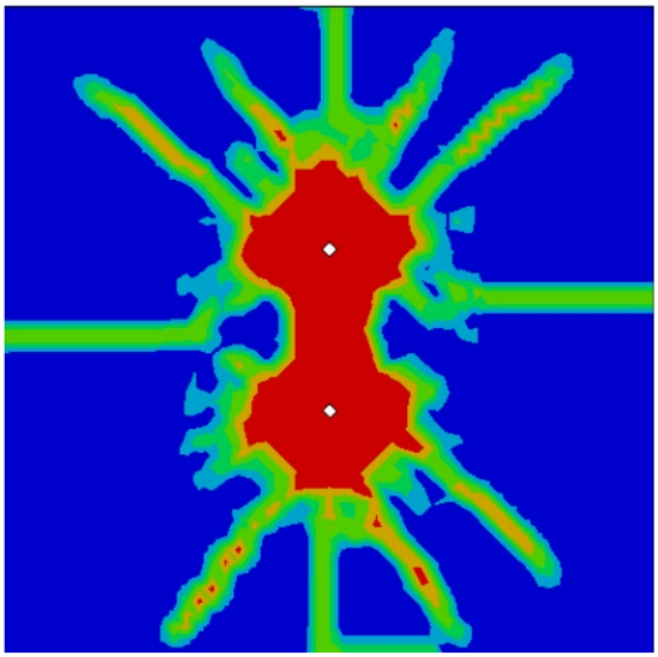

Figure 54 Damage Pattern for Vertical Blasthole Spacing of 0.5m

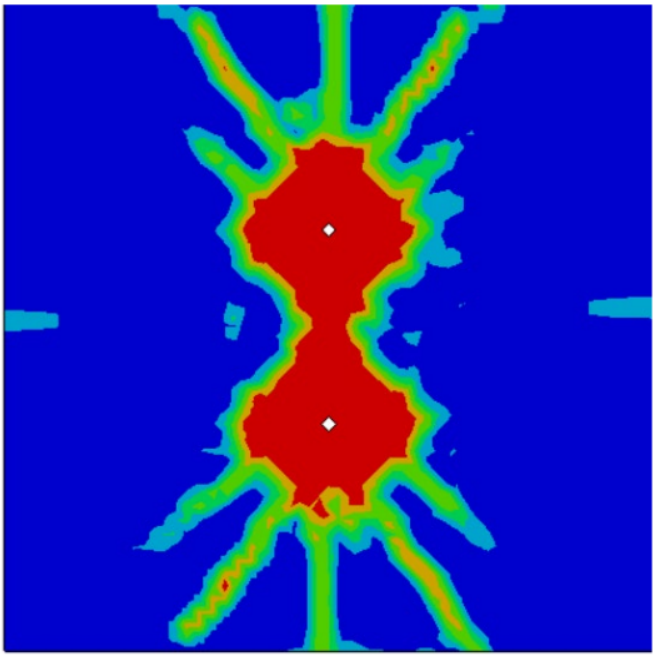

Figure 55 Damage Pattern for Vertical Blasthole Spacing of 0.6m

It can be seen from Figures 44 to 55 that as the spacing between the blastholes increased, the damage zone extended in the direction parallel to the explosives for both the horizontal and vertical spacings of blastholes. For shorter distance between the blastholes, the stress waves generated by both the blastholes interacted resulting in larger damage around the blastholes. With the increase in spacing, there is lesser interaction between the stress waves. There was lesser superposition of stress waves compared to smaller spacings and there was an extension of damage zone but lesser damage.

6. CONCLUSION

The comparison of the numerical model to the results of the laboratory experiment served two purposes. Firstly, it helped to calibrate the model for further simulations of the effect of decoupling coefficients and effect of blasthole spacing. Secondly, it helped to compare two common constitutive models for simulating the brittle behavior of rock materials, JH-2 model and RHT model.

Both JH-2 model and RHT model are efficient in simulating the cracks compared to a laboratory experiment. However, more cracks comparable to the experiment were found with the RHT model. Therefore, the RHT model is better compared to the JH-2 model.

The effect of decoupling ratio was investigated using the calibrated model. RHT model was used for the rock. The result clearly showed in terms of damage to the rock and the pressure in the blasthole that as the decoupling coefficient increased, the damage to the rock decreased. It indicates that there is dissipation in the blast wave pressure through the coupling media. It is an essential finding in controlled blasting which can help in understanding the effect of air media for optimizing the blast design. Furthermore, a comparison was made between two decoupling medias commonly used in explosion, air, and water. **It was found that in terms of energy dissipation, air is a better decoupling media than water. The pressure transmitted to the surrounding rock by water as a decoupling media is 2-3 times higher than when the air is used as the decoupling media.**

The delay time between explosives detonation is another essential parameter. **It was found that there is an optimum delay time for different spacings of boreholes as shown by the increasing damage up to that delay time and decrement in crushed area of rock beyond that delay time. It can be useful for calculating the delay timings of explosives.**

In addition, it was found that as the spacing increases the damage increases in the direction parallel to the explosives for both the horizontal and vertical spacing of explosives. For shorter distance between the blastholes, the stress

waves generated by both the blastholes interacted resulting in larger damage around the blastholes. With the increase in spacing, there is lesser interaction between the stress waves. There was lesser superposition of stress waves compared to smaller spacings and there was an extension of damage zone but lesser damage.

REFERENCES

Banadaki, M. (2010). Stress-wave induced fracture in rock due to explosive action. *Doctoral Dissertation University of Toronto*.

Borrvall T, R. W. (2011). The RHT Model in LS DYNA. *In: Proceedings of the 8th European LS-DYNA users conference, Strasbourg*.

Ding, Y. L. (2021). Fractal damage and crack propagation in decoupled charge blasting. *Soil Dynamics and Earthquake engineering*.

Fakhimi A, L. M. (2014). DEM-SPH simulation of rock blasting. *Computers and Geotechnics:45*, 158-164.

Jayasinghe, S. Z. (2019). Numerical investigation into the blasting induced damage characteristics of the rocks considering the role of in-situ stress and discontinuity persistence. *Computer and Geotechnics*.

Johnson, G. a. (1992). A Computational Constitutive Model for Brittle Materials Subjected to Large Strains. *Shock wave and High Strain Rate Phenomena in Materials, edited by M.A. Meyers, L.E. Murr and K.P. Staudhammer , Marcel Dekker, Inc , New York*, 1075-1081.

Li, L. Q. (2023). Numerical study on fracture control blasting using air-water blasting. *Geomech.Geophys.Geo-energ.Geo-resour.*

LSTC. (2007). Retrieved from https://ftp.lstc.com/anonymous/outgoing/jday/manuals/ls-dyna_971_manual_k_rev1.pdf

Ma, L. Y. (2022). Study on energy evolution and crack propagation of rock mass under single hole uncoupled charge blasting. *Applications in Engineering Science 11*.

Riedel W, T. K. (1999). Penetration of Reinforced Concrete by BETA-B-500, Numerical Analysis using a New Macroscopic Concrete model using hydrocodes. *Proceedings of International Symposium on Interaction of the Effects of Munitions with Structures, Berlin*, 315-322.

Song, L. G. (2019). Study on the Decoupled Charge Effect in the deep hole cumulative blasting of coal seam. *Advances in civil Engineering, 2019*.

Tao, Y. L. (2020). Numerical investigation of blast-induced rock fragmentation. *Computers and Geotechnics 128*.

Ucar, R. (1975). *Decoupled explosive charge effects on blasting performance.* Retrieved from https://scholarsmine.mst.edu/masters_theses/3034

Wang. (2018). Numerical Simulations of rock blasting damage based on laboratory scale experiments. *Journal of Geophysics and Engineering*.

Wang, W. L. (2020). Explosion propagation and characteristics of rock damage in decoupled charge blasting based on computed tomography scanning. *International Journal of Rock Mechanics and Mining Sciences*.

Wang, W. W. (2021). Finite element analyses of constitutive models performance in the simulation of blast-induced rock cracks. *Computers and Geotechnics 135.*

Xie, L. L. (2017). Analysis of damage mechanisms and optimization of cut blasting design under high in-situ stresses. . *Tunnel and Underground Space Technology*, 19-31.

Yang, D. Y. (2018). Visualizing the blast-induced stress wave and blasting gas action using digital image correlation. *International Journal of Rock Mechanics and Mining Sciences*, 47-54.

Yi, S. P. (2017). A numerical study of impact of short delays on rock fragmentation. *International Journal of Rock Mechanics and Mining Sciences 100*, 250-254.

APPENDICES

PROCEDURES FOR FINITE ELEMENT ANALYSIS

Define Material Property for Explosives.

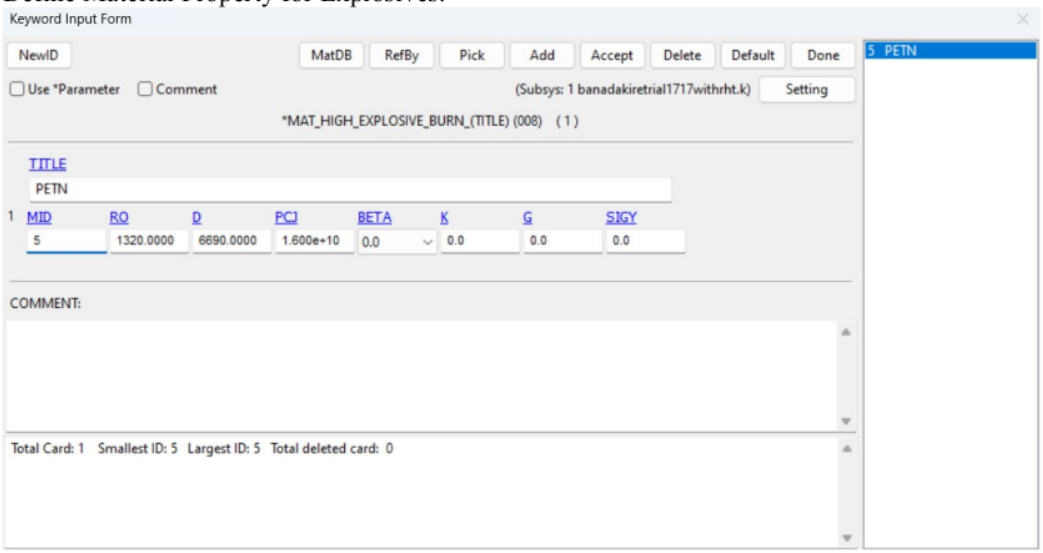

Define Material Property for Air.

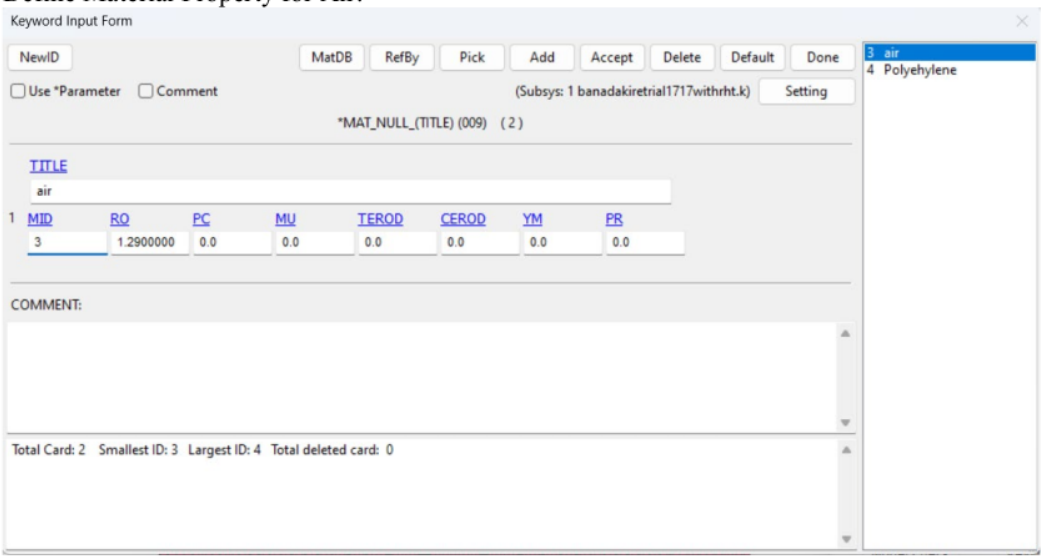

Define Polyethylene Material.

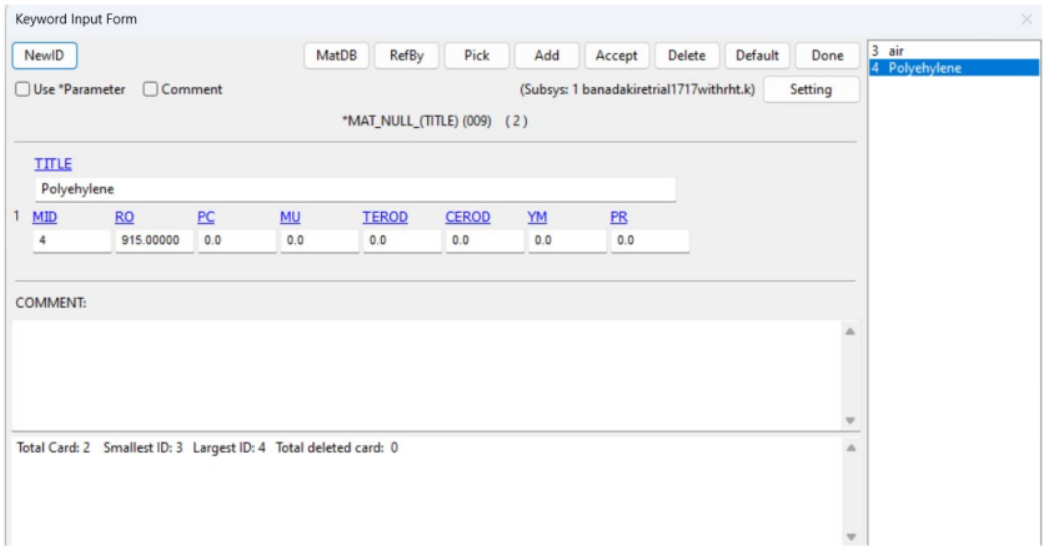

Define Copper Material.

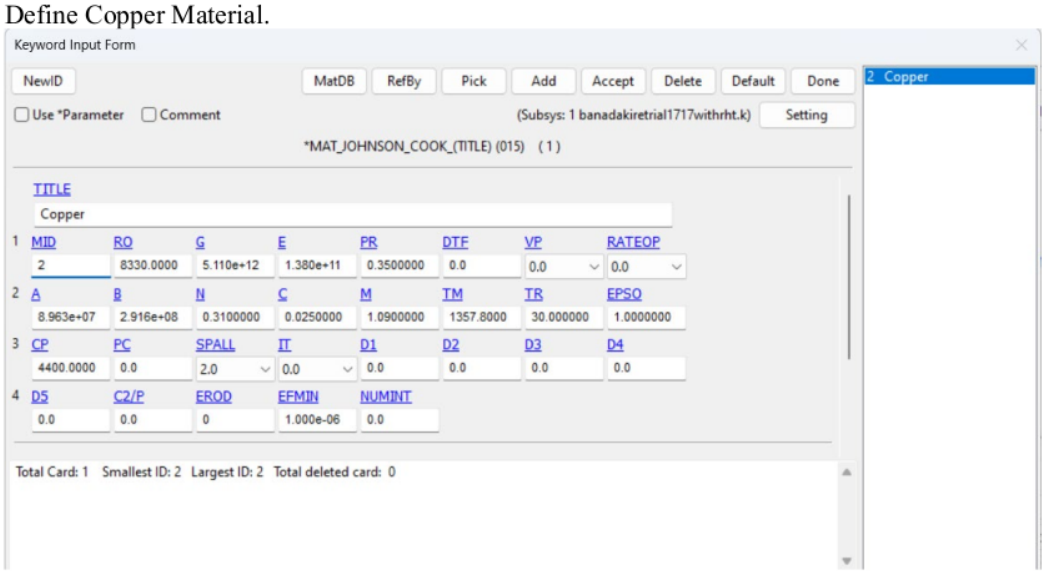

Define Rock Material.

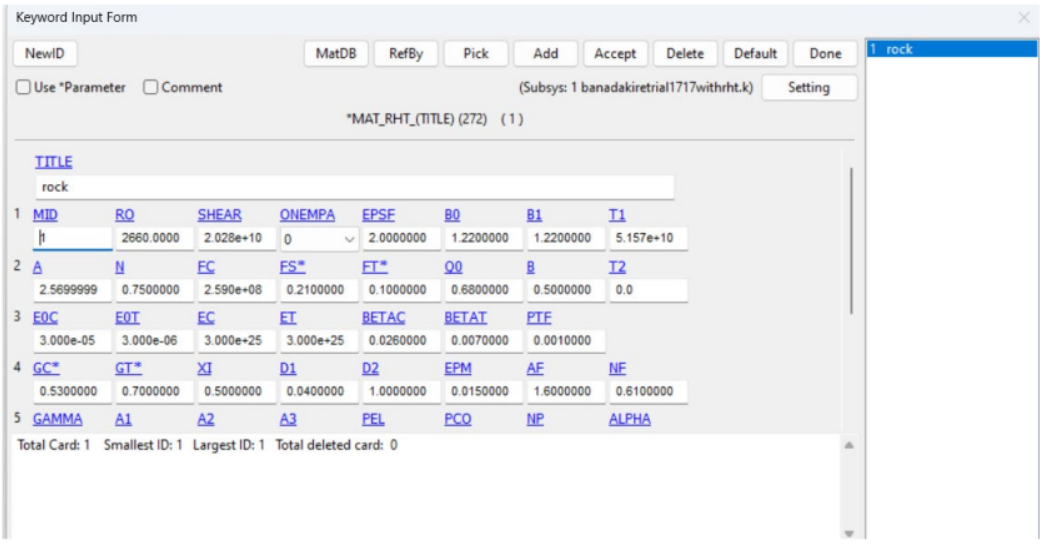

Define Equation of State for Copper.

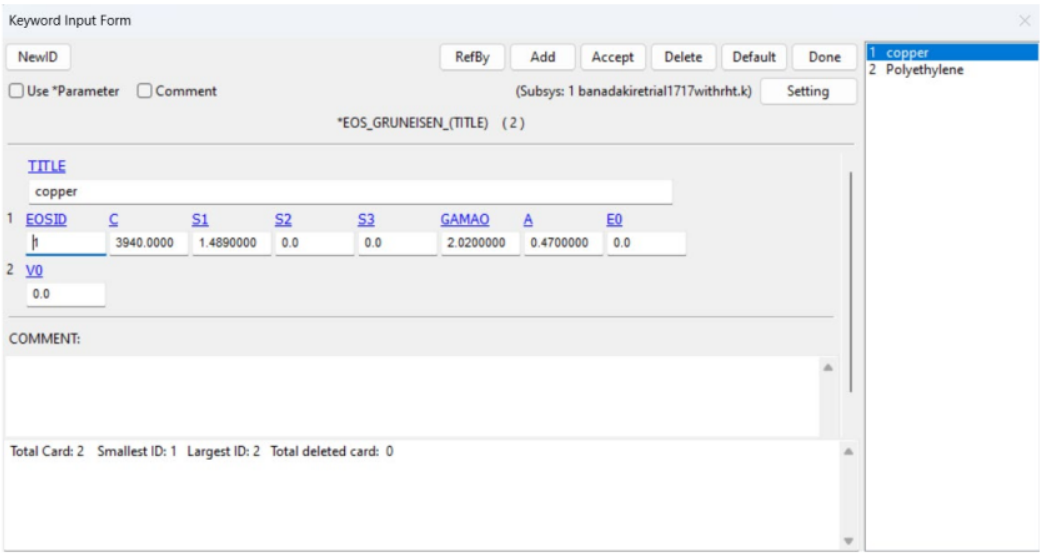

Define Equation of State for Polyethylene.

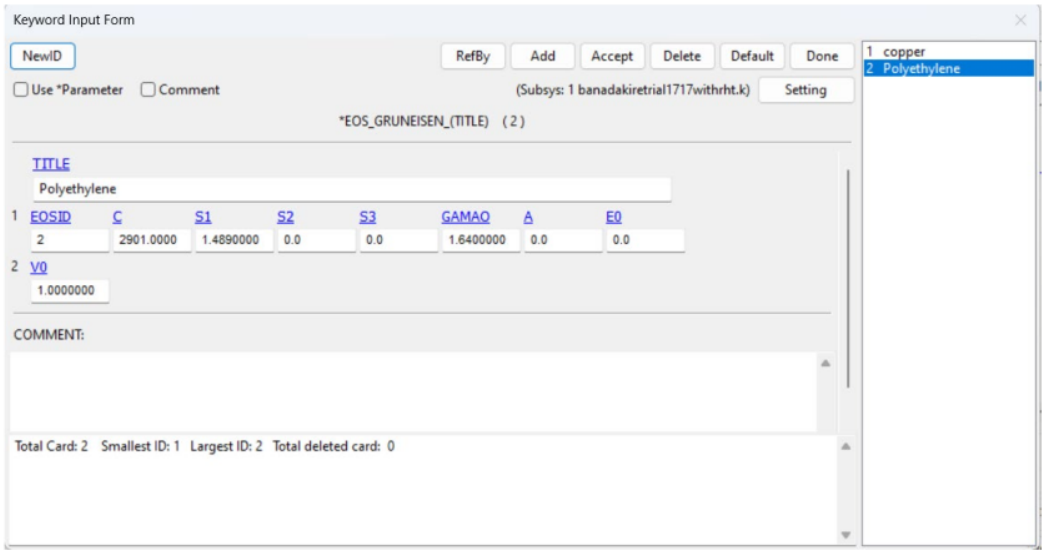

Define Lagrange Section.

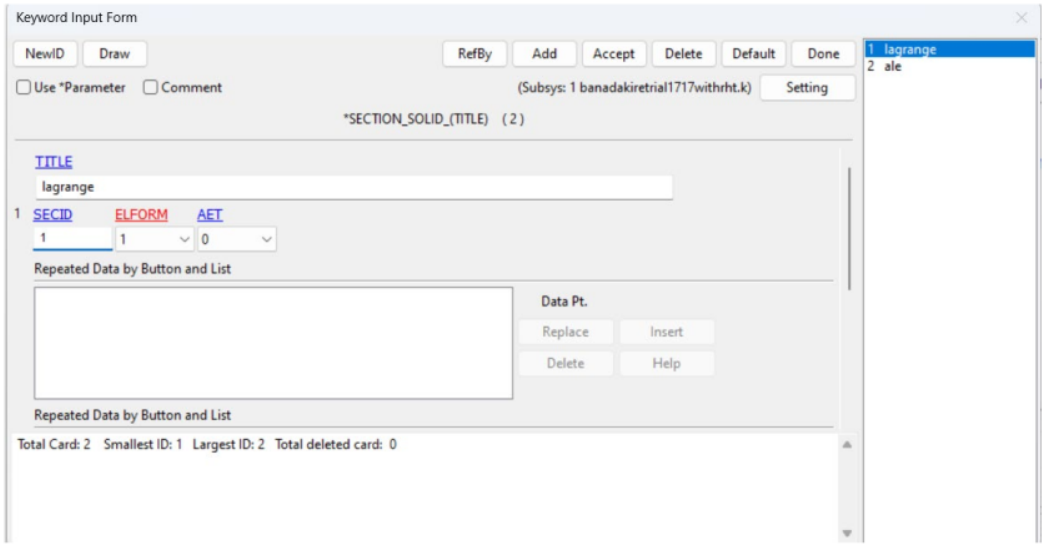

Define ALE Section.

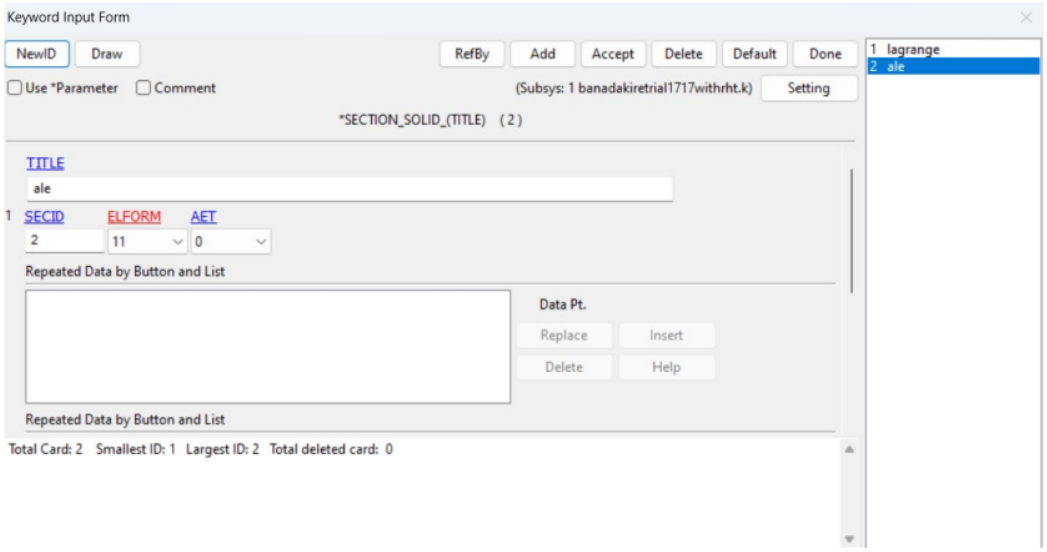

Define Lagrange and ALE Hourglass.

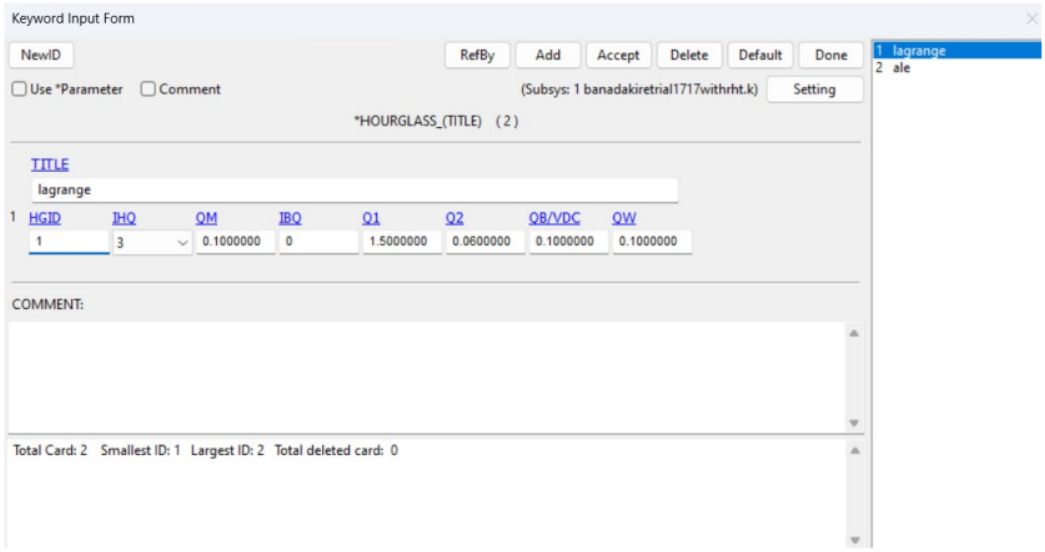

Assign Material and Section Property to Rock.

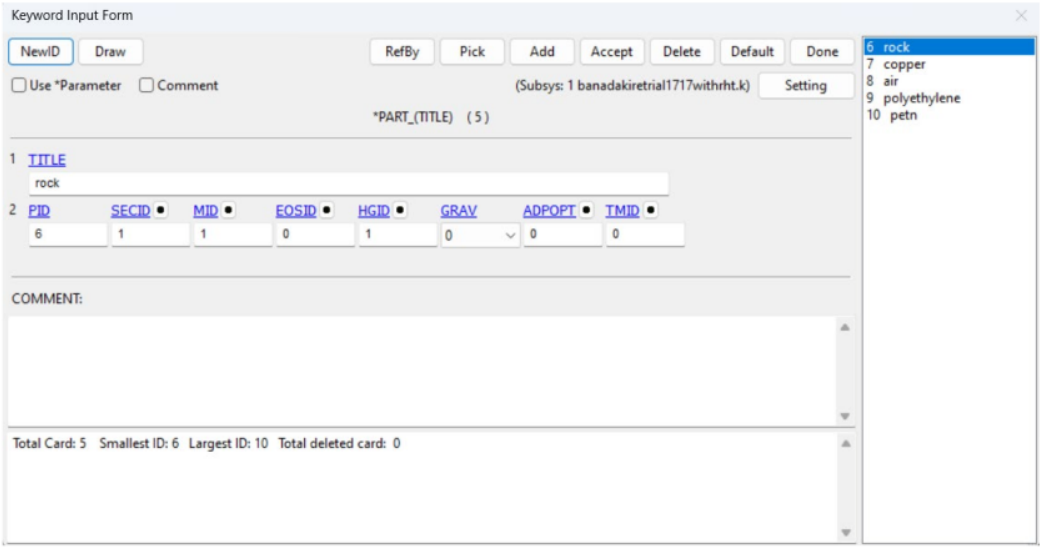

Assign Material and Section Property to Copper.

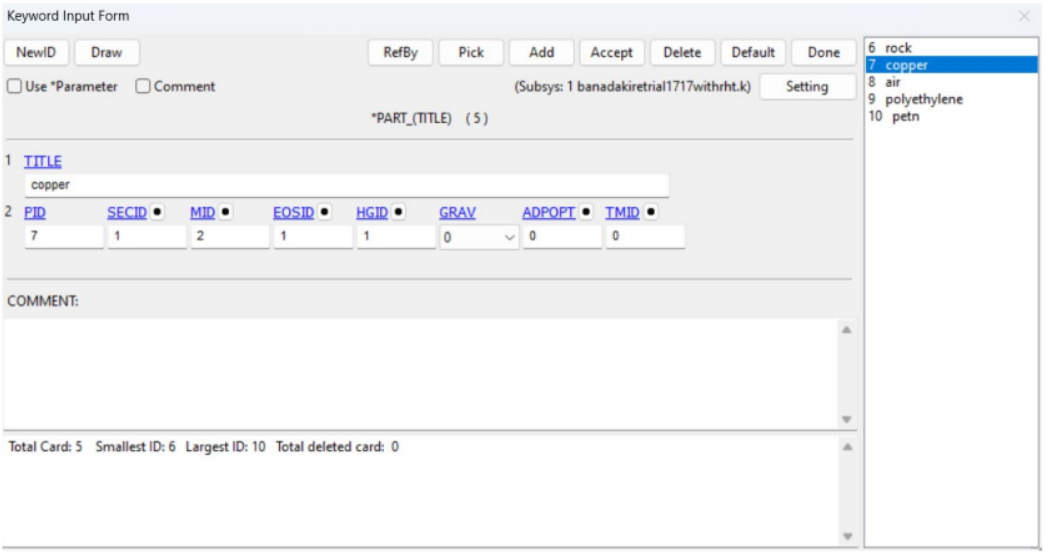

Assign Material and Section Property to Air.

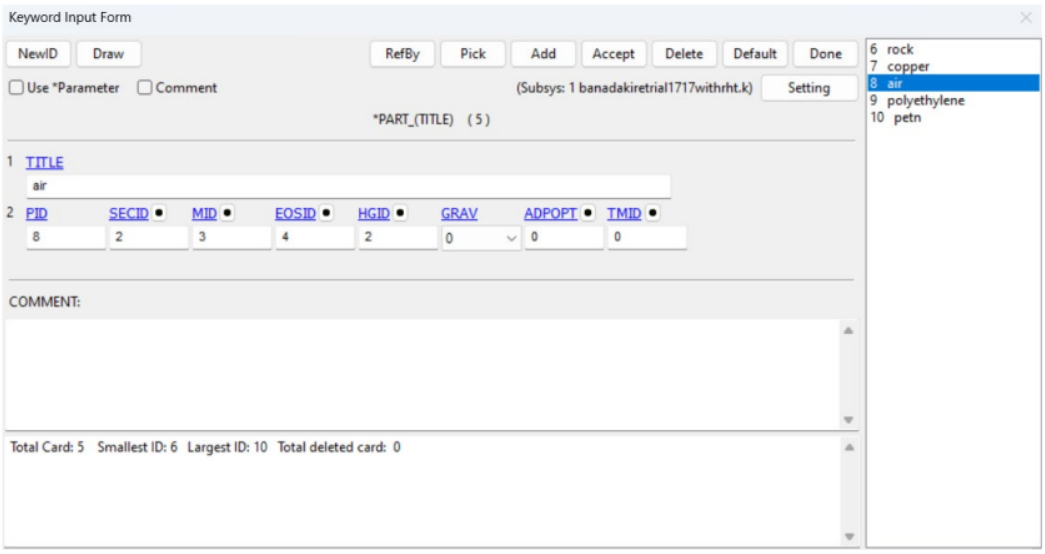

Assign Material and Section to Polyethylene.

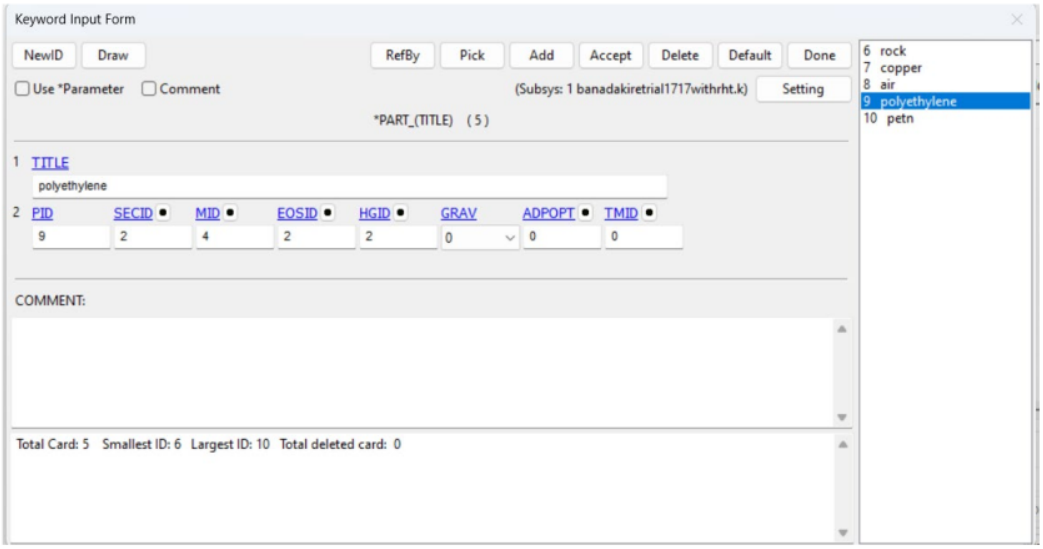

Assign Material and Section to Explosive.

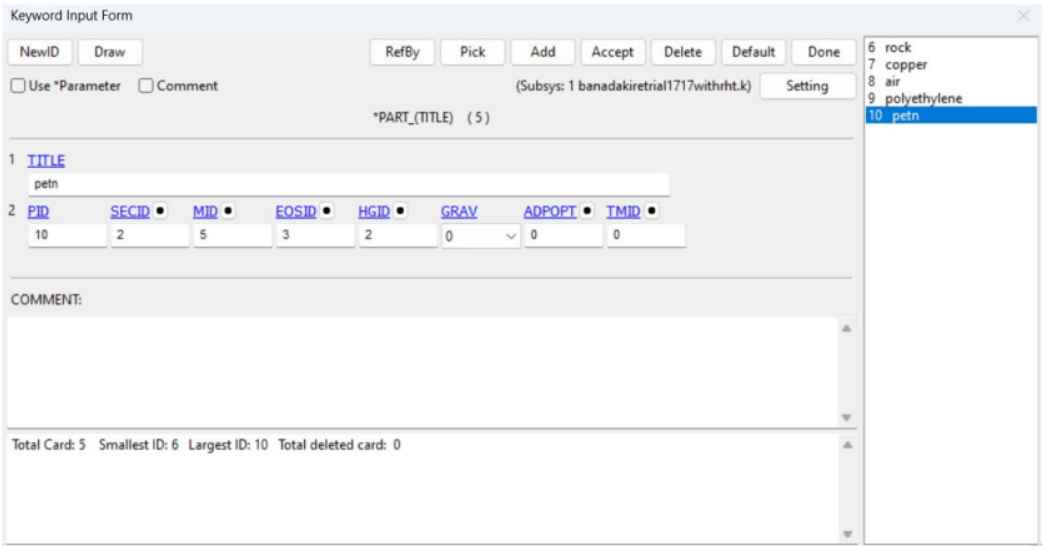

Define Lagrange and ALE Part List.

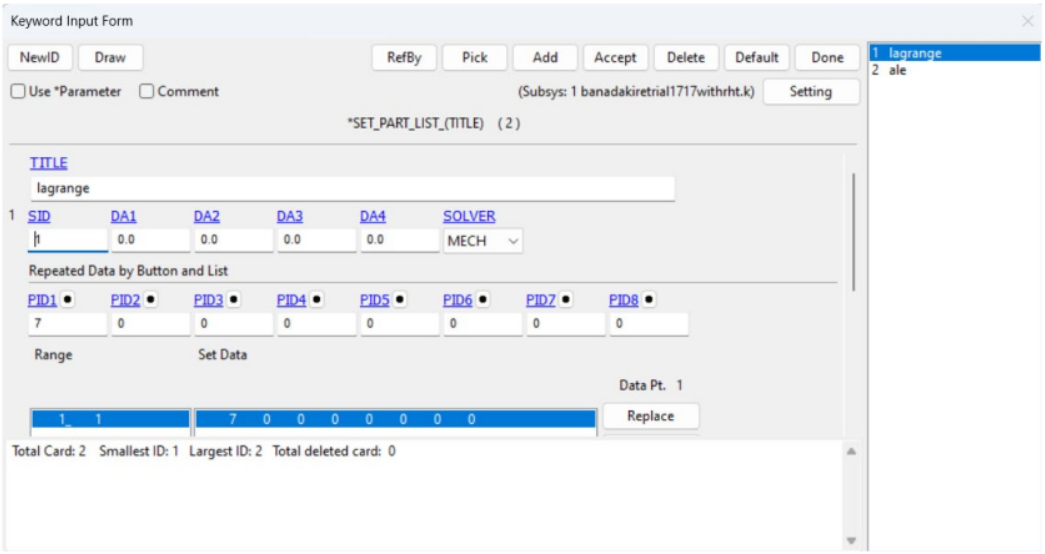

Define ALE Multimaterial Group.

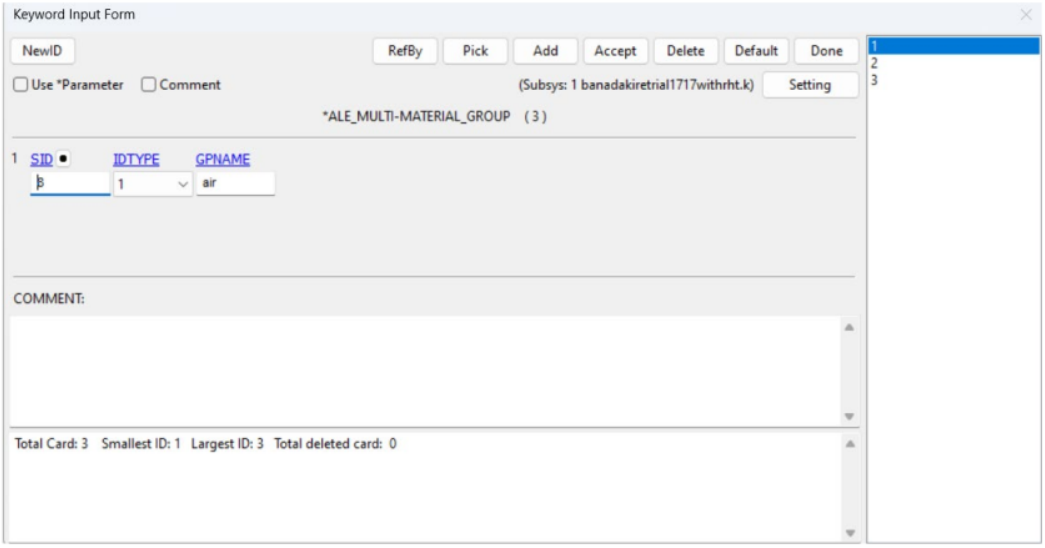

Define AMMG for Polyethylene.

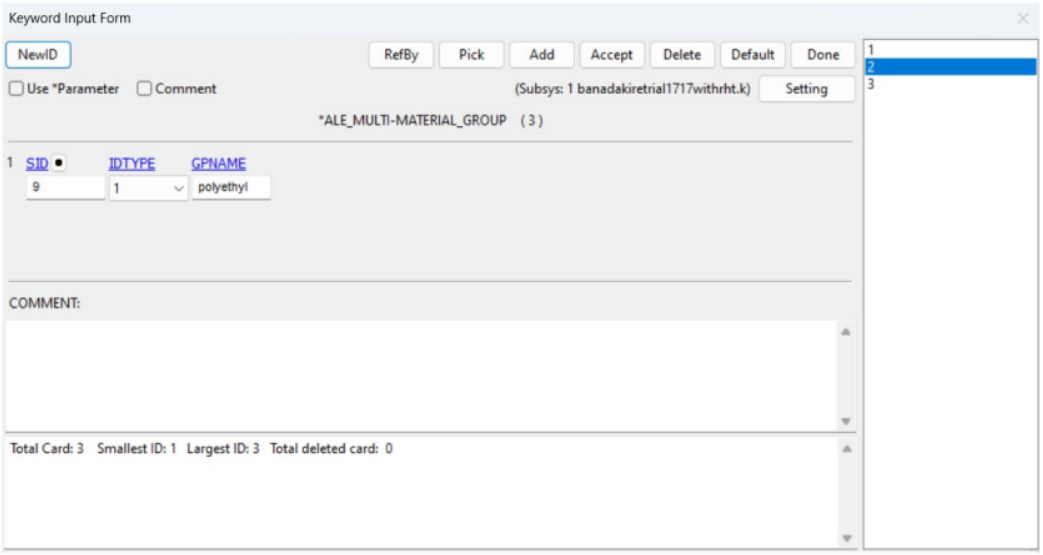

Define AMMG for PETN and Air.

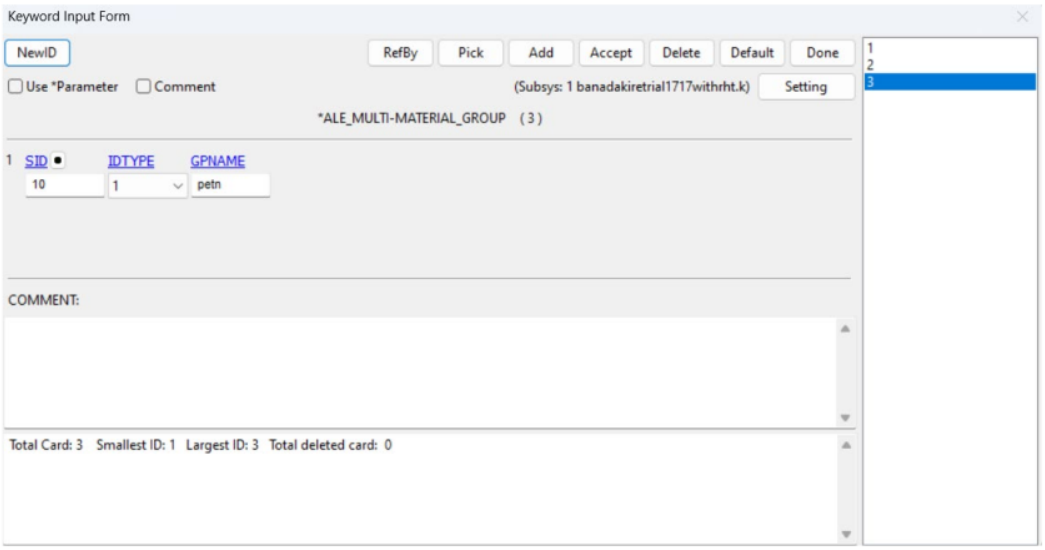

Assign Coupling between Lagrangian and ALE entities.

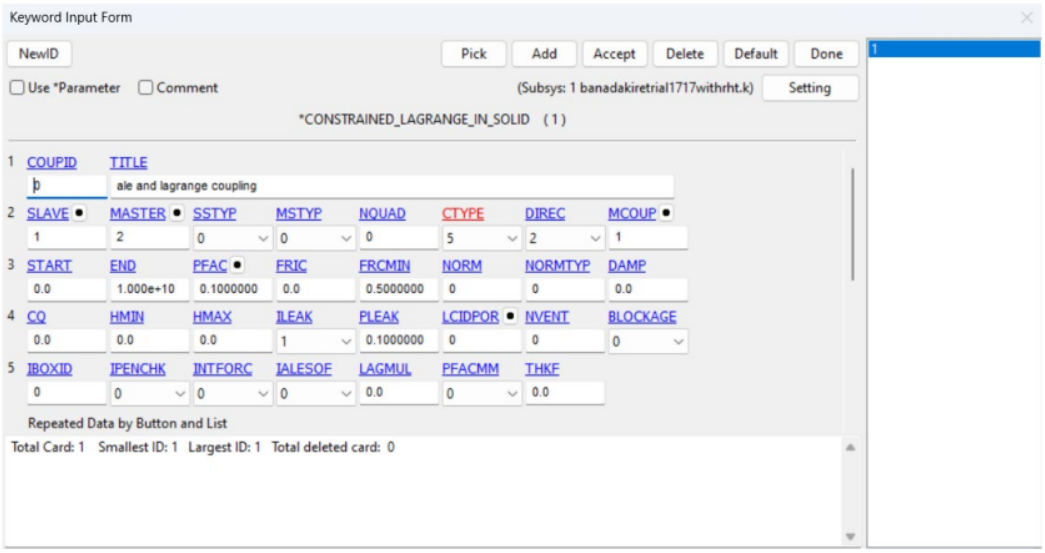

Define ALE parameters.

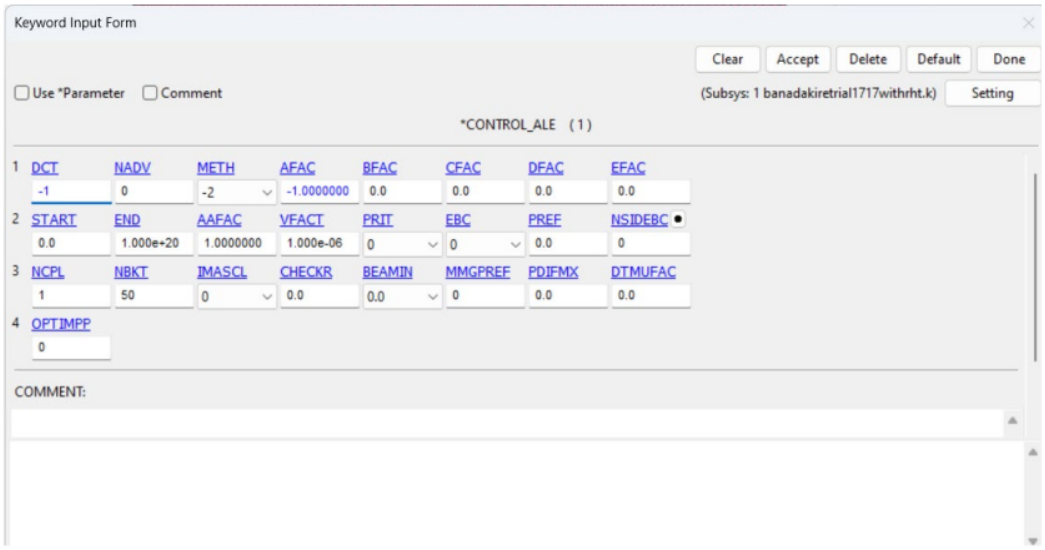

Assign Termination time.

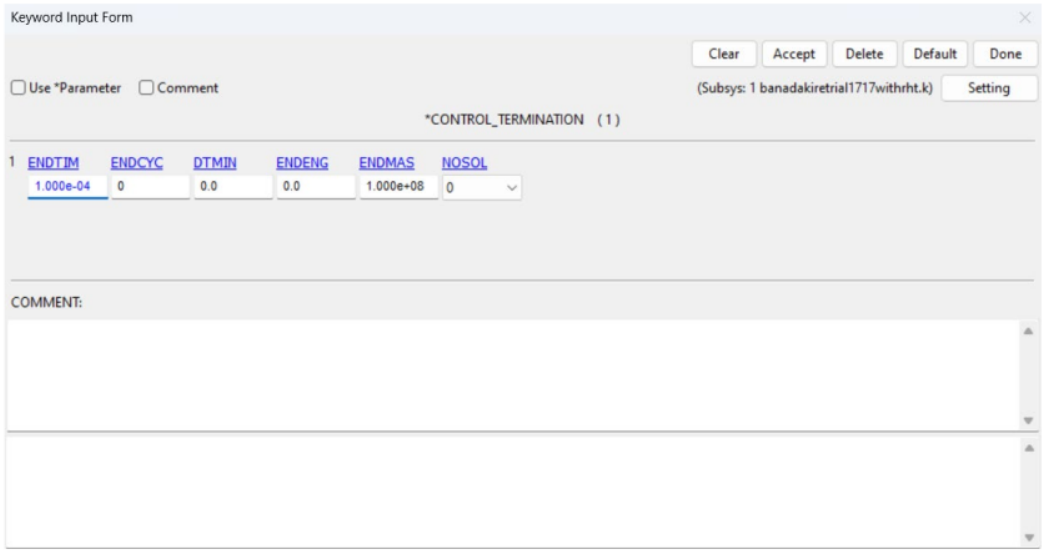

Define timescale and mass scaling factors.

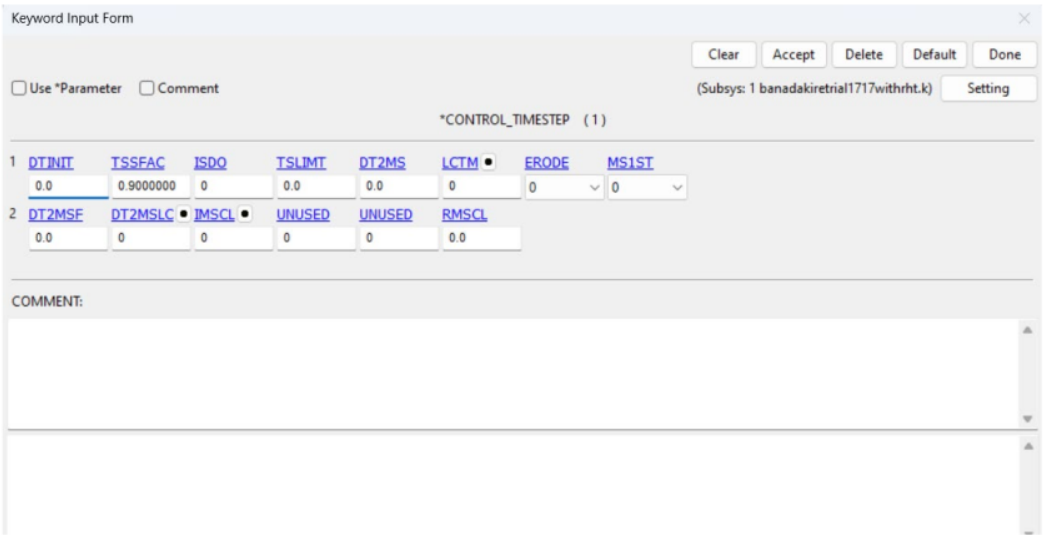

Define time period between the outputs.

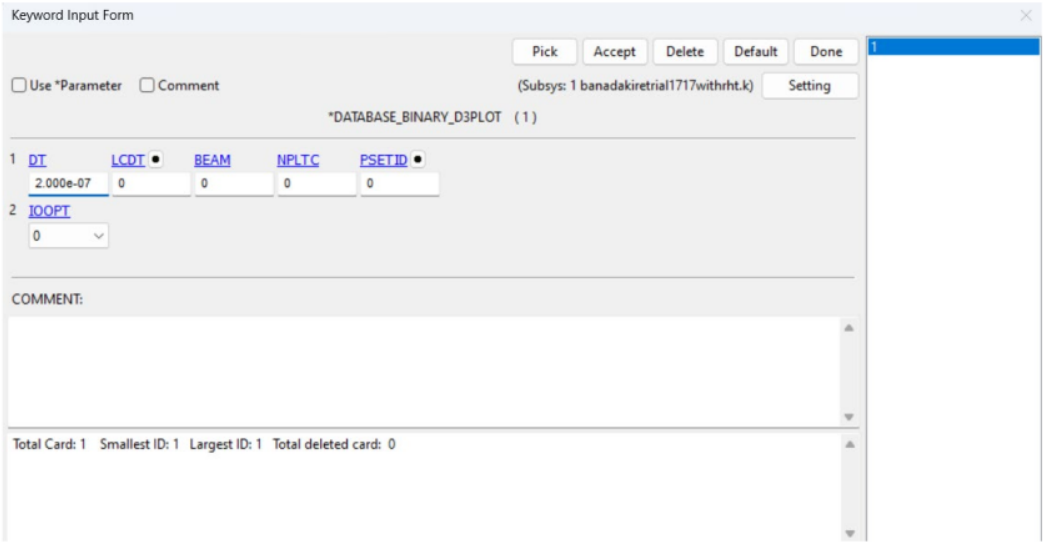

Assign Time interval between the outputs.

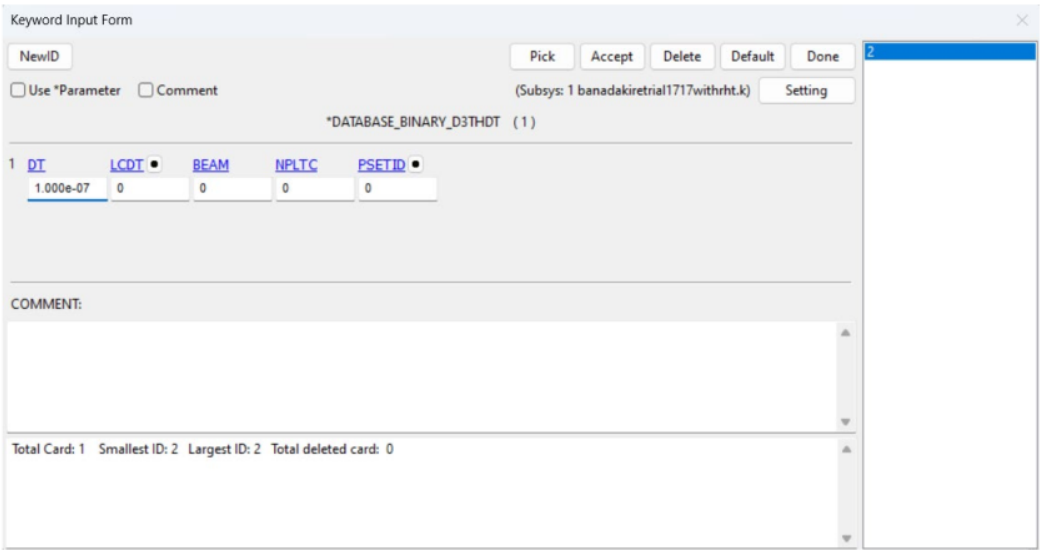

Define output characteristics.

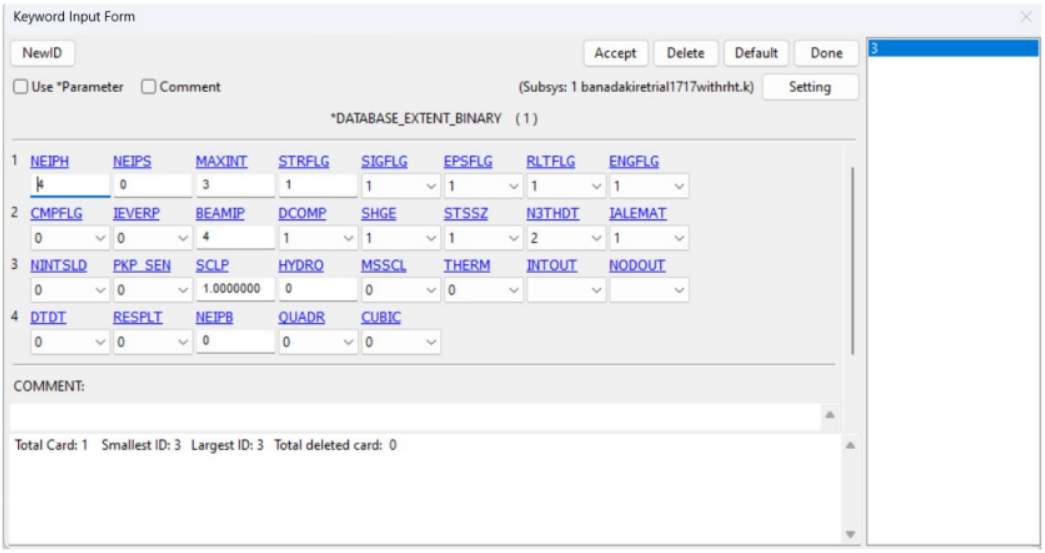

Assign explosives and coordinates.

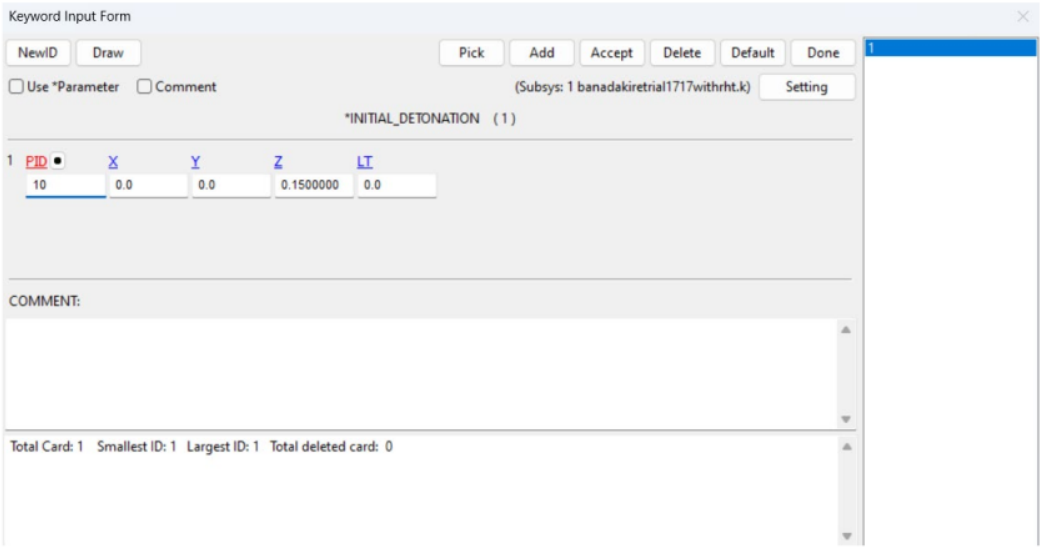
Keyword Input Form
NewID
Draw
Pick
Add
Accept
Delete
Default
Done
Use *Parameter
Comment
(Subsys: 1 banadakiretrial1717withrht.k)
Setting
*INITIAL_DETONATION (1)
1
PID
X
Y
Z
LT
10
0.0
0.0
0.1500000
0.0
COMMENT:
Total Card: 1 Smallest ID: 1 Largest ID: 1 Total deleted card: 0
1

NUMERICAL ANALYSIS OF ROCK BLASTING

ORIGINALITY REPORT

14%
SIMILARITY INDEX

PRIMARY SOURCES

1	academic.oup.com Internet	171 words — 1%
2	elibrary.tucl.edu.np Internet	167 words — 1%
3	www.hindawi.com Internet	136 words — 1%
4	ascelibrary.org Internet	131 words — 1%
5	Dehghan Banadaki, Mohammad M. "Stress-wave induced Fracture in Rock due to Explosive Action", Proquest, 2012. ProQuest	113 words — 1%
6	core.ac.uk Internet	112 words — 1%
7	Zhixian Hong, Ming Tao, Xuejiao Cui, Chengqing Wu, Mingsheng Zhao. "Experimental and numerical studies of the blast-induced overbreak and underbreak in underground roadways", Underground Space, 2022 Crossref	74 words — 1%
8	www.researchgate.net Internet	73 words — 1%

9	eprints.qut.edu.au Internet	60 words — < 1%
10	conference.ioe.edu.np Internet	36 words — < 1%
11	dhapdam.gov.np Internet	36 words — < 1%
12	C. C. Liao, Yaguang Wang, Jinjian Chen, Qi Zhang. "Parametric study for underwater blast-induced pipeline response embedded in marine sediments", Marine Georesources & Geotechnology, 2018 Crossref	34 words — < 1%
13	www.mdpi.com Internet	32 words — < 1%
14	Xudong Jiang, Yiguo Xue, Fanmeng Kong, Huimin Gong, Yusong Fu, Weimeng Zhang. "Dynamic responses and damage mechanism of rock with discontinuity subjected to confining stresses and blasting loads", International Journal of Impact Engineering, 2022 Crossref	28 words — < 1%
15	Feli, S.. "Finite element simulation of ceramic/composite armor under ballistic impact", Composites Part B, 201106 Crossref	26 words — < 1%
16	Koneshwaran, Sivalingam, Thambiratnam, David, Gallage, Chaminda. "Performance of buried tunnels subjected to surface blast incorporating fluid structure interaction", 'American Society of Civil Engineers (ASCE)', 2015 Internet	21 words — < 1%
17	tase23.artun.ee Internet	

21 words — < 1%

18 qspace.library.queensu.ca
Internet
19 words — < 1%

19 ltu.diva-portal.org
Internet
18 words — < 1%

20 Zhongqi Wang, Guangdong Gong, Yanchun Zhang, Chunhua Bai. "Simulation of the response of glass window under blast load", Transactions of Tianjin University, 2008
Crossref
17 words — < 1%

21 Ruishan Cheng, Wensu Chen, Hong Hao, Jingde Li. "Dynamic response of road tunnel subjected to internal Boiling liquid expansion vapour explosion (BLEVE)", Tunnelling and Underground Space Technology, 2022
Crossref
16 words — < 1%

22 C.P. Yi, E. Nordlund, P. Zhang, S. Warema, S. Shirzadegan. "Numerical modeling for a simulated rockburst experiment using LS-DYNA", Underground Space, 2020
Crossref
15 words — < 1%

23 Jianxiu Wang, Yao Yin, Kamran Esmaieli. "Numerical Simulations of Rock Blasting Damage Based on Laboratory Scale Experiments", Journal of Geophysics and Engineering, 2018
Crossref
15 words — < 1%

24 kb.psu.ac.th
Internet
15 words — < 1%

25 Wang, Y.F.. "Finite element model of erosive wear on ductile and brittle materials", Wear, 20080825 — 14 words — < 1%
Crossref

26 Shenglin Li, Tianlong Ling, Dianshu Liu, Shufeng Liang, Rui Zhang, Bo Huang, Kai Liu. "Determination of Rock Mass Parameters for the RHT Model Based on the Hoek–Brown Criterion", Rock Mechanics and Rock Engineering, 2023 — 13 words — < 1%
Crossref

27 www.sciendo.com — 13 words — < 1%
Internet

28 Christoforou, C.C.. "Hyperbolic systems of balance laws via vanishing viscosity", Journal of Differential Equations, 20060215 — 12 words — < 1%
Crossref

29 Jiajun Ding, Jianhua Yang, Zhiwei Ye, Zhendong Leng, Chi Yao, Chuangbing Zhou. "Cut-Blasting Method Selection and Parameter Optimization for Rock Masses under High In Situ Stress", International Journal of Geomechanics, 2023 — 12 words — < 1%
Crossref

30 Roshan Vijay Marode, Srinivasa Rao Pedapati, Tamiru Alemu Lemma, Venkata Somi Reddy Janga. "Thermo-Mechanical Modelling of Friction Stir Processing of AZ91 Alloy: Using Smoothed-Particle Hydrodynamics", Lubricants, 2022 — 12 words — < 1%
Crossref

31 Yiping Zhang, Yi Luo, Sipeng Wan, Yingxiang Tian, Huanchao Ding, Xiaoxiao Zhang, Chengcheng Fang, Yuyao Zhang. "Influence of Decoupled Charge Structure and Filler on the Blasting Effect", Shock and Vibration, 2020 — 12 words — < 1%

Crossref

32 www.scribd.com
Internet
12 words — < 1%

33 Hao Zhang, Tingchun Li, Yiteng Du, Qingwen Zhu, Xiantang Zhang. "Theoretical and numerical investigation of deep-hole cut blasting based on cavity cutting and fragment throwing", Tunnelling and Underground Space Technology, 2021
Crossref
11 words — < 1%

34 Jiliang Kan, Linming Dou, Xuwei Li, Jiazhuo Li, Jinzheng Bai, Jinrong Cao, Minghong Liu. "Effect of initiation pattern on rock damage and blasting seismic under multi-hole blasting", Geomatics, Natural Hazards and Risk, 2023
Crossref
11 words — < 1%

35 Taotao Wang, Ansheng Cao, Weiliang Gao, Guangyong Wang, Xiaowang Sun. "Damage Evolution and Circumferential Strain Distribution Characteristics of the Bolt-Supported Cavern under Multiple Explosion Sources", Shock and Vibration, 2021
Crossref
11 words — < 1%

36 ftp.eq.uc.pt
Internet
11 words — < 1%

37 Chahmi Oucif, J.S. Kalyana Rama, K. Shankar Ram, Farid Abed. "Damage modeling of ballistic penetration and impact behavior of concrete panel under low and high velocities", Defence Technology, 2020
Crossref
10 words — < 1%

38 Jiang-Tao Zhang, Li-Sheng Liu, Peng-Cheng Zhai, Zheng-Yi Fu, Qing-Jie Zhang. "The prediction of
10 words — < 1%

the dynamic responses of ceramic particle reinforced MMCs by using multi-particle computational micro-mechanical method", Composites Science and Technology, 2007
Crossref

39 Lee, Chi-Seung, Myung-Sung Kim, Kwang-Ho Choi, Myung-Hyun Kim, and Jae-Myung Lee. "Numerical Prediction Method for Elasto-Viscoplastic Behavior of Glass Fiber Reinforced Polyurethane Foam Under Various Compressive Loads and Cryogenic Temperatures", Volume 3 Structures Safety and Reliability, 2015.
Crossref
10 words — < 1%

40 M.G Cottrell, J. Yu, D.R.J. Owen. "The adaptive and erosive numerical modelling of confined boron carbide subjected to large-scale dynamic loadings with element conversion to undeformable meshless particles", International Journal of Impact Engineering, 2003
Crossref
10 words — < 1%

41 Ma, G.W.. "Numerical simulation of blasting-induced rock fractures", International Journal of Rock Mechanics and Mining Sciences, 200809
Crossref
10 words — < 1%

42 Michał Kucewicz, Paweł Baranowski, Łukasz Mazurkiewicz, Jerzy Małachowski. "Comparison of selected blasting constitutive models for reproducing the dynamic fragmentation of rock", International Journal of Impact Engineering, 2022
Crossref
10 words — < 1%

43 Mingchao Du, Zengliang Li, Xiangwei Dong, Guanan Hao, Xiaopeng Du, Jiaqi Che, Yanwen Zhang. "Experiment and simulation study of erosion mechanism in float glass due to rhomboid particle impacts", International Journal of Impact Engineering, 2020
Crossref
10 words — < 1%

44	Sivalingam Koneshwaran, David P. Thambiratnam, Chaminda Gallage. "Blast Response of Segmented Bored Tunnel using Coupled SPH–FE Method", Structures, 2015 Crossref	10 words — < 1%
45	Xudong Li, Kewei Liu, Tao Qiu, Yanyan Sha, Jiacai Yang, Ruitao Song. "Numerical study on fracture control blasting using air–water coupling", Geomechanics and Geophysics for Geo-Energy and Geo-Resources, 2023 Crossref	10 words — < 1%
46	apps.dtic.mil Internet	10 words — < 1%
47	eprints.nottingham.ac.uk Internet	10 words — < 1%
48	spiral.imperial.ac.uk Internet	10 words — < 1%
49	www.dynalook.com Internet	10 words — < 1%

EXCLUDE QUOTES	ON	EXCLUDE SOURCES	< 10 WORDS
EXCLUDE BIBLIOGRAPHY	ON	EXCLUDE MATCHES	< 10 WORDS